TAILORING OF POLYMER-NANOMATERIAL INTERACTIONS

By

LAWANYA RAJ OJHA

Bachelor of Science
Tribhuvan University
Kirtipur, Kathmandu, Nepal
1996

Master of Science
Western Illinois University
Macomb, IL
2007

Submitted to the Faculty of the
Graduate College of the
Oklahoma State University
in partial fulfillment of
the requirements for
the Degree of
DOCTOR OF PHILOSOPHY
December, 2012

TAILORING OF POLYMER-NANOMATERIAL INTERACTIONS

Dissertation Approved:

Dr. Kevin D. Ausman

Thesis Adviser

Dr. Frank D. Blum

Dr. Ziad El Rassi

Dr. Barry K. Lavine

Dr. Ali K. Kalkan

Dr. Sheryl A. Tucker

Dean of the Graduate College

ACKNOWLEDGEMENTS

First and most importantly, I would like to thank deeply my advisor Prof. Kevin D. Ausman for giving me this opportunity to finish this exciting research. Working with Dr. Ausman has been tremendously rewarding. His guidance and insightfulness in a plethora of subject helped me to resolve many problems encountered with this work. I am always thankful to him for giving me absolute freedom to work on problems and approaches of my interest.

I also would like to thank the member of my advisor committee Prof. Frank D. Blum, Prof. Ziad El Rassi, Prof Barry K. Lavine and Prof. Ali K. Kalkan for taking time out of their hectic schedules to read my thesis and be on my defense committee.

I would like to thank my collaborators Prof. Raman Singh, Prof. Ali K. Kalkan and Prof. Ranji Vaidyanathan from the College of Engineering, Architecture and Technology, Oklahoma State University, Stillwater/Tulsa, OK. Fracture toughness measurement and helium gas permeability measurements presented in chapter III have been done in the group of Prof. Singh by Kunal Mishra and Sadia Nashrin respectively. Raman spectroscopy analyses have been carried out in the group of Prof. Kalkan by Sriharsha Karumuri. DMA analysis presented in chapter III was performed in the Prof. Vaidyanathan group by K. Lakshminarayanan.

I am forever grateful for my dad, mom and my brother Achyut for their long-standing support and patience in the completion of my Ph.D. I also want to express my gratitude to my son Avash. Last but not least I would like to deeply thank my beloved wife Anita who is always on my side, taking care of me and loving me a lot. I love you forever.

TABLE OF CONTENTS

Chapter Page

1. INTRODUCTION 1
1.1. Nanomaterials 1
1.2. Polymer Nanocomposites 2
1.3. Nanomaterials for Polymeric Nanocomposite 2
1.4. Challenges Involved in Preparing Nanocomposites 4
1.5. Importance of Polymer-Nanomaterial Interaction 5
1.6. This Dissertation 5

2. BACKGROUND 7
2.1. Carbon Nanotubes 7
2.1.1. Structure of Carbon Nanotubes 8
2.1.2. Synthesis of Single-Walled Carbon Nanotubes 10
2.1.3. Characterization of Single-Walled Carbon Nanotubes 12
2.1.4. Dispersion of Single-Walled Carbon Nanotubes 17
2.2. Polyhedral Oligomeric Silsesquioxanes 23
2.2.1. Synthesis of Polyhedral Oligomeric Silsesquioxanes 24
2.2.2. Hybrid Properties of Polyhedral Oligomeric Silsesquioxanes 26
2.2.3. Polyhedral Oligomeric Silsesquioxanes in Nanocomposites 27
2.2.4. Polyhedral Oligomeric Silsesquioxanes in Epoxy Nanocomposites 29

3. EXPERIMENTAL SECTION 31
3.1. Materials 31
3.2. Instrumentation 32
3.3. Procedure 35

4. DISPERSION OF SINGLE-WALLED CARBON NANOTUBES BY ENCAPSULATION IN A LINEAR CROSSLINKABLE POLYMER 43
4.1. Dispersion of Single-Walled Carbon Nanotubes 43
4.1.1. SDS Assisted Dispersion of Single-Walled Carbon Nanotubes 43
4.1.2. PVP Assisted Dispersion of Single-Walled Carbon Nanotubes 45
4.2. Stability of Dispersion of Single-Walled Carbon Nanotubes 47
4.2.1. PVP-PAAm Assisted Dispersion of Single-Walled Carbon Nanotubes 48
4.2.2. Crosslinking of Polymer and Verification of Crosslinking 50
4.2.3. Stability of Single-Walled Carbon Nanotubes Dispersion after Crosslinking of PVP-PAAm 52

5. EPOXY/POLYHEDRAL OLIGOMERIC SILSESQUIOXANE NANOCOMPOSITES 56
5.1. Synthesis and Curing of Epoxy/POSS Nanocomposites 56
5.2. Characterization of Epoxy/POSS Nanocomposites 58
5.2.1. Differential Scanning Calorimetry (DSC) Studies 58
5.2.2. Dynamic Mechanical Analysis(DMA) 59
5.2.3. Fracture Toughness 63
5.2.5. Helium Gas Permeability 66

5. CONCLUSION 69

REFERENCES 71

LIST OF TABLES

Table Page

Table 3.1. Properties of EPON 862 40
Table 3.2. Properties of glycidyl POSS cage mixture 41

LIST OF FIGURES

Figure Page

2.1 van Hove singularities of metallic (a) and semiconducting SWNTs (b). 14
2.2 Possible polymer wrapping arrangement of PVP on SWNTs. 22
2.3 Hybrid properties of POSS 27
3.1 Structure of some crosslinkable copolymers of PVP.....37
3.2 Structure of DGEBF (a), IPDA (b) and glycidyl POSS (c) 41
4.1 Fluorescence spectra under 658 nm laser excitation of SWNTs dispersions in aqueous SDS solution at different sonication energy 44
4.2 AFM images of SWNTs dispersion a) after 60 kJ b) 120 kJ ultrasonic energy introduced to the samples 45
4.3 Fluorescence spectra of SWNTs dispersions at different stages of the procedure before and after the addition of PVP 47
4.4 Fluorescence spectra of SWNT upon addition of PVP-PAAm at a) 658 nm b) 782 nm excitation wavelength 49
4.5 Fluorescence spectra taken at 658 nm excitation wavelengths during the removal of surfactant and excess of polymer after polymer wrapping on SWNTs 50
4.6 Crosslinking of PVP-PAAm by glutaraldehyde 51
4.7 UV-Vis absorption spectra of glutaraldehyde-crosslinked polymer.....51
4.8 SWNT fluorescence spectra taken at 658 nm excitation while dispersed in SDS (black), after the SDS has been replaced by PVP-PAAm (red), after crosslinking with GLU (blue), and after adding THF to the suspension (green). .53
4.9 Vis-NIR absorbance of SWNTs in SDS (A), Polymer wrapped SWNTs before (B) and after crosslinking (C) 54
4.10 AFM image of polymer wrapped SWNTs after crosslinked by GLU 55
5.1 Raman spectra of DGEBF and POSS 57
5.2 Raman spectra of epoxy/POSS composites after post curing at 200^{o}C 57
5.3 DSC curves for various epoxy/POSS composites 59
5.4 Plot of Storage modulus vs temperature for epoxy/POSS composites 60
5.5 Loss modulus vs temperature curves for various epoxy/POSS composites 61
5.6 Tan delta curves for various epoxy/ POSS composites 62
5.7 Comparison of T_g as determined by DSC and DMA 62
5.8 Fracture toughness value in term of critical intensity factors for different loading of POSS in epoxy/POSS composites 63
5.9 SEM micrographs of epoxy/POSS composites (a) neat resin (b) 1 wt.% POSS loading (c) 5wt.% POSS loading.....65

5.10 SEM micrographs of epoxy/POSS composites (a) 1 wt. % POSS loading (b) 5 wt. % POSS loading. Arrows point the formation of voids 66
5.11 Helium gas permeability coefficient for epoxy composites for different POSS loading 68

CHAPTER 1

INTRODUCTION

This thesis is concerned with the tailoring of polymer-nanomaterial interaction. I begin the thesis with brief introduction of nanomatrials, polymer nanocomposites and polymer nanomaterial interaction. This chapter provides the brief introduction of the context of the work and the structure of the thesis.

1.1. Nanomaterials

Nanomaterials are those materials that have at least one dimension measuring 1 to 100 nm.[1] They include nanoparticles, nanotubes, nanofibers, etc. The size of the nanomaterials falls between that of individual atoms or molecules and the corresponding bulk materials.materials. Size reduction can modify the physical and chemical properties of nanomaterials distinctively from their bulk counterparts.[2] Nanomaterials have greater surface area per mass than bulk materials, which allows more atoms or molecules to be exposed on the surface so that adjacent atoms and molecules can interact more readily. As a result, nanomaterials are attractive for variety of applications such as fillers, catalysts, drug delivery, semiconductors, microelectronics, and cosmetics.[3]

1.2. Polymer Nanocomposites

A material that is made from two or more physically distinct phases to achieve better properties than either single homogeneous component is called a composite material. Generally composite materials are composed of fillers that act as reinforcing material dispersed within a continuous matrix to bind the fillers. In polymer composite materials, any of a variety of fillers, such as metalic, organic, and inorganic particles are dispersed in a polymer matrix. When nanomaterials are used as fillers the composite material is termed a polymeric nanocomposite. The properties of nanocomposites depend not only on the bulk properties of each of the components as in the case with conventional macrocomposites, but also on the nature of interactions between the two phases as well as the interphases between them. For nanocomposites, the interactions between the polymer and nanofiller have a much greater effect on the composite properties than for conventional macrocomposites at the same volume fraction of fillers because of the very large surface area of the nanofiller. As a result, there is a possibility of tremendous improvement in the properties of polymers with the addition of nanofillers.[4-8] Therefore, nanocomposites are promising high-performance and lightweight materials for many applications including spacecraft structures, automobile structures, and sporting goods.[9-13]

1.3. Nanomaterials for Polymeric Nanocomposite

There are three kinds of nanomaterials used in polymer nanocomposites. Depending upon the number of dimensions that are not confined to a nanoscale range,

they are classified as two dimensional, one dimensional and zero dimensional nanomaterials.

When two of the dimensions are not confined to the nanoscale range, they are called two dimensional nanomaterials. These materials are sheets of one to a few nanometers thick, but have lengths and widths that are often hundreds to thousands nanometers. Layered silicates (nanoclays) and exfoliated graphite are good examples of such materials. Both nanoclays and graphite have been widely investigated as nanofillers to improve mechanical, thermal, optical and physiochemical properties.[12-16]

Fillers with two dimensions confined to the nanometer size scale are considered to be one dimensional nanomaterials. Since the third dimension is larger, these materials form elongated structure such as carbon nanotube, nanofibers and cellulose whiskers. Such materials have been extensively studied as reinforcing nanofillers to achieve exceptional properties.[6,17-20] However, carbon nanotubes have shown little success as a filler for polymer nanocomposites despite the superior properties of the nanotubes themselves. They are very expensive and often exhibit significant aggregation due to strong interactions (0.5 eV/nm) between the pristine nanotubes and weak interaction with the surrounding matrix.

Finally, zero dimensional nanomaterals have all three dimensions in the nanometer range. Spherical silica nanoparticles and polyhedral oligomeric silsesqiuoxanes (POSS) are good examples of this category.[21-24] These nanoparticles offer advantages over one dimensional and two dimensional nanoparticles because of their smaller size. When these nanoparticles are dispersed as individual particles, they have the potential to act as

molecular reinforcements in polymer composites without requiring a significant alteration to processing conditions.

1.4. Challenges Involved in Preparing Nanocomposites

Because of their typically high surface energy, nanomaterials often exist as aggregates that are very difficult to disperse in a liquid or in a solid medium. Because such a dispersed state is usually not a thermodynamic equilibrium, the use of nanofillers in a polymer matrix is often challenging because of this agglomeration, making the properties of such systems very difficult to explore.[25,26] Approaches such as ultasonication and high shear mixing are frequently used to facilitate dispersion, although the effectiveness of these approaches is limited by the reaggregation of the nanoparticles as the system shifts toward the equilibrium, phase-separated state. Stabilizing agents such as surfactants can make the dispersed state metastable, which in turn can lengthen the time the dispersed state is usable. These stabilizing agents can overcome the attractions between the nanoparticles either by the formation of electrical double layer or by steric interaction between them.[27] However, if left in the mixture during composite formation, these stabilizing agents often degrade the composite's ultimate properties, and thus are usually desirable to avoid. Hence an imperative challenge for researchers is to explore alternative techniques to achieve individually-dispersed nanomaterials in polymer matrices.

1.5. Importance of Polymer-Nanomaterial Interaction

Polymer assisted dispersion of nanomaterials could be an alternative approach to preparing polymer nanocomposites. Polymers can easily adsorb to the surface of nanomaterials and act as stabilizers to prevent aggregation. Steric interactions between the adsorbed polymer chains provides the strong repulsion between the two approaching surfaces of the nanomaterial. The polymer assisted dispersion technique is simple, economic, and more ecofriendly than traditional techniques. Polymer coated nanoparticles can be designed to be compatible with the polymer matrix of interest, and often preserves the composite's ultimate properties. However, while this approach opens new doors for the application of nanomaterials in nanocomposites, there are still some challenges to developing this processing technique at an industrial scale. These fundamental challenges include understanding the polymer nanomaterial interaction to stabilize non-aggregated nanomaterials in the polymer matrix and developing polymer-coated nanomaterials that can be used as nanofillers in polymer nanocomposites at affordable cost. The research reported here has focused on the interactions of polymers with two different kinds of nanomaterials: (a) single-walled carbon nanotubes (SWNTs) and (b) polyhedral oligomeric silsesquioxanes (POSS).

1.6. This Dissertation

The research described in this dissertation encompasses two distinct projects. Both of these projects focus on the interactions between nanomaterials and associated organic polymers; however, the two projects are distinct enough that separate results and discussion sections will be included for each project.

Chapter 2 provides the necessary background relevant to the contents of the thesis. It discusses the two different kinds of nanomaterials, SWNTs and POSS, and describes the various procedures for their synthesis and characterization. Chapter 3 describes the experimental methods and materials used for these studies. Chapters 4 and 5 contain the results and discussion of these two different projects separately. Chapter 4 discusses the first project, "Dispersion of single-walled carbon nanotubes by encapsulation in a linear crosslinkable polymer." Chapter 5 discusses "Epoxy/polyhedral oligomeric silsesquioxanes nanocomposites." The overall conclusions of this thesis are summarized in chapter 6.

CHAPTER 2

BACKGROUND

This chapter provides background materials concerning carbon nanotubes and polyhedral oligomeric silsesquioxanes. For the SWNTs, I describe their classification, structure, synthesis, characterization techniques, and dispersion processes. For POSS, I describe their structure, synthesis, and applications.

2.1. Carbon Nanotubes

Carbon nanotubes (CNTs), discovered in 1991 by Ijima,[28] have attracted intense attention due to their exceptional promise as materials for a variety of applications because of their superior electronic, mechanical, optical, and structural properties.[29-32] Because of the small diameters of CNTs (typically from 0.7-3 nm for single walled carbon nanotubes), they become quasi one-dimensional in terms of their mechanical and electronic properties. Isolated CNTs are light-weight and have the highest tensile modulus (~1 TPa) of any known fiber.[33] CNTs are also thermally stable at temperatures of more than 1000 ^{o}C in an inert atmosphere and have a thermal conductivity similar to diamond.[34] They are potential candidates for chemical applications such as catalysis and energy storage because of their hollow center and high surface area.[35-37] Other

remarkable properties of CNTs include their electronic and optoelectronic properties.[38-43] In particular, CNTs can be either metallic or semiconducting depending on their chirality.[44,45] Since metallic single-walled carbon nanotubes have extremely high electrical conductivities compared even to copper wire, they have been used to make conductive thin films, transparent electrodes, and nanowires. On the other hand semiconducting nanotubes are promising for high-performance field-effect transistors, organic photovoltaic cells, and organic light emitting diodes. The existence of both electrical types of nanotubes has raised hopes for future applications of CNTs in many types of nanoelectronics.[46-55]

2.1.1. Structure of Carbon Nanotubes

CNTs are allotropes of carbon. They are ultrathin carbon fibers with nanometer-scale diameters and up to micrometer-scale lengths. Structurally, they can be viewed as rolled-up graphene sheets, although this visualization doesn't reflect their synthesis methods. All the carbon atoms in underivatized carbon nanotubes are sp^2 hybridized. There are two main structural types of CNTs: those with a single layer are called single-walled carbon nanotubes (SWNTs) while those with nested multiple layers are called multi-walled carbon nanotubes (MWNTs). MWNTs are easier to produce in bulk quantities than SWNTs; however, the structure of MWNTs is less well-defined because of their greater complexity and variety and their greater propensity to have defect sites. Although they are harder to synthesize, particularly in bulk quantities, SWNTs have better mechanical and electrical properties than MWNTs, making SWNTs more attractive for many applications. In the present work, I will only discuss single-walled carbon nanotubes.

SWNTs can be conceptually viewed as a cylindrical tubes formed by rolling of a single layer of graphene. The crystal structure of SWNTs depends upon the axis along which the cylinder is rolled from the graphene sheet, which is specified by the chiral vector or roll-up vector (C_h). This vector defines the relative location of the two sites on the graphene sheet that, upon rolling, become coincident. It is specified by a pair of integers (*n, m*) that relate C_h to the two unit vectors $\mathbf{a}_1$ and $\mathbf{a}_2$ by following equation.[56]

$$\boldsymbol{C}_h = n\mathbf{a}_1 + m\mathbf{a}_2$$

The angle between the chiral vector and the nearest unit vector is known as chiral angle (θ), resulting in possible values that range between 0 to 30^o. The axis of the tube lies perpendicular to the chiral vector. The set of all pairs of non-negative integers where n≥m encompass all unique SWNTs structures. When the components *n* and *m* are equal, the chiral angle is at its maximum of 30^o, resulting in what are called "armchair" structures because of the similarity of a cross-section of the tube perpendicular to the tube axis to the shape of an armchair. When *m*=0 the chiral angle is at its minimum of 0^o, resulting in nanotubes that are termed "zigzag" structures, again because of the cross-sectional shape of the tube. All other kinds of SWNTs are chiral with the helical hexagonal path along the chiral vector.

The (*n, m*) designation of SWNTs determines their electronic properties, based on their differing boundary conditions perpendicular to the tube axis. All arm chair structures of SWNTs (*n*=*m*) are metallic because they have finite density of states at the fermi energy level. Other SWNTs structures where *n*-*m* is evenly divisible by 3 are semi metallic and the remaining SWNTs structure where *n*-*m* is not divisible by 3 are semiconductors.

2.1.2. Synthesis of Carbon Nanotubes

Carbon nanotubes are synthesized by extracting carbon atoms from a carbon carrying precursor. Originally solid state carbon precursors were used to provide the carbon source needed for nanotube growth; however, much work has also been done to synthesize CNTs by catalytic decomposition of carbon-containing gaseous on transition metal catalysts. Some of the common synthesis methods of CNTs are described briefly below.

2.1.2.1. Arc-Discharge Method

The arc discharge method is the oldest and easiest methods to produce CNTs, and is still extensively used.[57,58] Although this method is very simple, the final product contains mixtures of components such as fullerenes, graphite, amorphous carbon, and metal catalysts along with CNTs. It requires extensive purification to separate CNTs from remaining materials present in the crude product. In this method CNTs are created through the electric-arc vaporization of two graphite electrodes, separated by an approximately 1 mm gap of an inert atmosphere. A direct current of 50 to 100 A passed through the electrodes creates high temperature discharge within the gap and vaporizes the surface of one of the electrodes. As a result CNTs deposit on the surface of other electrode. CNTs synthesized by this method have a narrow diameter (~ 1.4 nm), but tend to have higher defect densities than those produce by some other methods.

2.1.2.2. Laser Ablation Method

In this method, developed by the Smalley group in 1996,[59] SWNTs are produced by laser vaporization of a graphite rod that contains a 1:1 mixture of cobalt and nickel catalyst in an oven at 1200 ^{o}C in flowing helium or argon gas. As the vaporized species

cools down, carbon atoms and small molecules quickly condense to form fullerenes. Where the catalyst is attached to the carbon clusters, it prevents the closing of the fullerene cage, thereby allowing the growth of carbon nanotubes from the catalyst as more carbon deposits. This growth continues, templated by the already-growing nanotubes, until the catalyst particles become too large or cool to the point that they no longer allow the continued growth. CNTs are obtained in long crystalline ropes with average diameter of 10-20 nm, with the individual tubes having an average diameter of 1.4 nm.

2.1.2.3. Chemical Vapor Deposition

In this process, CNTs are synthesized by flowing high-temperature carbon-containing gases across a stationary metal catalyst.[60-63] Several different carbon-containing compounds have been used as precursors such as methane, carbon monoxide, acetylene, ethylene, benzene, and methanol.[64-68] Each gas has a particular decomposition temperature, thereby resulting in a different required nanotube growth temperature, which can range from 550 ^{o}C to 1000 ^{o}C. The active catalytic species are transition metal nanoparticles such as Fe, Ni, Co, Mo, Cu, and Au. This process has ability to grow well-separated, long single-walled carbon nanotubes with a variable defect density and low amorphous carbon content.

One particularly effective variant of this method, known as CoMoCat, was developed by the Resasco group in 1999 at the University of Oklahoma.[70,71] This is also a catalytic method to produce SWNTs of high quality and with a remarkably narrow distribution of diameter. In this method SWNTs are grown by the disproportionation of CO on bimetallic Co-Mo/SiO_2 (silica supported Cobalt and Molybdenum) catalyst at

700-950 ^{o}C in a flow of CO at pressure 1-10 atm. This process is also used for bulk production of SWNTs.

2.1.2.4. High Pressure Carbon Monoxide Process

The high pressure carbon monoxide process (HiPco) was developed by the Smalley group in 1999 for the bulk production of SWNTs.[69] This technique is a catalytic production of SWNTs in a continuous flow gas phase process using CO as a carbon feedstock and iron pentacarbonyl $Fe(CO)_5$ as the iron-containing catalytic precursor. SWNTs are produced by flowing CO, mixed with small amount of $Fe(CO)_{5,}$ at a pressure of 1-10 atm and a temperature of 800-1200 ^{o}C through a reactor. Size and diameter distribution of SWNTs can be roughly selected by controlling the pressure of CO. The average diameter SWNTs in HiPco under typical operating conditions is approximately 1 nm. The highest yields (~79%) can be achieved at the highest accessible temperature and pressure.

2.1.3. Characterization of Single-Walled Carbon Nanotubes

The chirality, electronic structure, and dispersion of SWNTs samples can be analyzed by examining their optical properties. Transmission electron microscopy (TEM) and atomic force microscopy (AFM) can be used to determine the length and diameter distributions of the nanotubes. Thermogravimetric analysis (TGA) reveals the amount of carbonaceous impurities and residual catalyst present in SWNTs samples.

2.1.3.1. Optical Properties of Single-Walled Carbon Nanotubes

The quasi-one dimensionality of SWNTs causes the electronic density of states to have a series of sharp van Hove singularities.[72,73] The energies between the van Hove singularities vary according to the nanotube diameter and (*n*, *m*) indices. The optical

absorption of a particular nanotube produces electronic transition between these singularities. These electronic transitions result in the characteristic absorption and emission properties of SWNTs.

2.1.3.1.1. Absorption Spectroscopy

Figure 1.1 shows a band theory model of the density of states for semiconducting and metallic SWNTs.[74] Each van Hove singularity belongs to a different sub band, labeled with an integer representing the magnitude of those states' angular momentum projection along the nanotube axis. The absorption spectra originate from electronic transitions from valance sub bands (v_1, v_2, v_3) to corresponding conduction sub bands (c_1, c_2, c_3, respectively). The absorption is relatively discrete and can be used to identify the types of SWNTs. Depending on the chiral vector of SWNTs, these interband transition (E_{ii}) have values ranging from 0.5 eV to 4 eV. For semiconducting SWNTs with diameter near 1 nm, the first three transitions S_{11}, S_{22}, and S_{33} will appear in the near-infrared, visible and near UV region respectively. Metallic SWNTs of similar diameters have their lowest energy optical transitions (M_{11}) in the visible region falling between semiconducting S_{22} and S_{33}. The absorption peaks are very useful in determining the (*n*, *m*) composition of a bulk SWNTs sample.

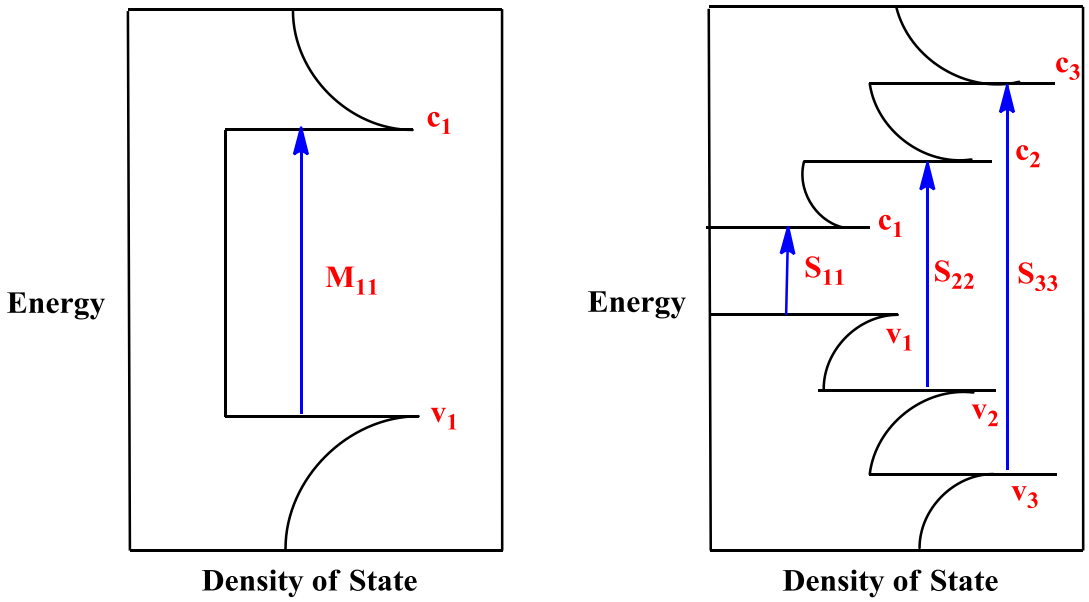

Figure 2.1. van Hove singularities of metallic (a) and semiconducting SWNTs (b).[74]

2.1.3.1.2. Band Gap Fluorescence

The discovery of band gap fluorescence from semiconducting SWNTs in aqueous surfactants suspensions allowed the quantitative determination of the concentrations of specific nanotube types by (*n*, *m*) index.[41] As was discussed above, semiconducting SWNTs of different (*n*, *m*) indices have distinct interband electronic transitions (S_{11}, S_{22}, S_{33}) between their van Hove singularities. Upon optical excitation of the second interband transition, an electron is excited from v_2 to c_2 by absorbing energy S_{22}, creating a hole in valence band v_2. Both electron and hole rapidly relax from c_2 to c_1 and v_2 to v_1 respectively. Thereafter, electron hole recombination takes place through the first van Hove transition (S_{11}) via fluorescence emission in the near-infrared region. As a result, light absorption at photon energy S_{22} is followed by florescence emission at S_{11}.[75]

Although electrons are exited from the valence band to the conduction band in metallic SWNTs, the continuous density of states through the Fermi level allows radiationless decay leading to electron/hole recombination. Further, energy and/or electron transfer between adjacent SWNTs can allow a metallic tube to quench the photoluminescence of semiconducting tubes. Thus, given that approximately one third of the tubes in any given sample are metallic, fluorescence is typically observed only for samples whose tubes have been isolated from each other.

2.1.3.1.3. Raman Spectroscopy

Raman spectroscopy is another powerful technique for SWNTs characterization. A strong resonantly-enhanced Raman signal can be obtained when the laser excitation energy is close to the energy between van Hove singularities in the valence and conduction bands. There are four important features in SWNTs Raman spectra: the Radial breathing mode (RBM), the disorder-induced mode (D-band), the tangential G-Mode (G-band) and the dispersive G' mode (G' or D* band).[76,77]

2.1.3.1.3.1. Radial Breathing Mode (RBM)

The radial breathing mode (RBM) arises from the scattering of light from the atomic vibration of nanotubes in the radial direction. They normally appear in the range of 100- 350 cm^{-1} for SWNTs of diameter range of 0.7 nm to 2 nm, and are considered to provide direct evidence of the presence of carbon nanotubes in a sample. The analysis of the RBM peaks provides information of SWNTs diameter in a sample. The RBM frequency is inversely proportional to the tube diameter (d) and is expressed by following equation.

$$\omega\mathrm{RBM} = \frac{A}{d} + B$$

Where A is constant of proportionality and B is interpreted as a damping of the environment surrounding the tube that depends on the tube-tube interactions. For an isolated SWNT on a SiO_2 substrate tends to have A= 248 cm^{-1} and B=0.[78] The RBM can be used to assign chirality of isolated SWNTs from a Kataura plot.[79]

2.1.3.1.3.2. Tangential G-Mode

The stretching of C-C bonds gives rise to G-band Raman feature that is common to all sp^2 carbon system. In carbon nanotubes the G-band is split into two peaks due to the curvature of the graphene sheet, one found near 1590 cm^{-1}(G^+) and the other near 1570 cm^{-1} (G^-). The G^+ band corresponds to vibrations along the nanotube axis and varies with charge transfer to or from the SWNTs. The G^- band corresponds to vibrations along the circumference of the SWNTs. The G^+ features of metallic and semiconducting SWNTs are found to show no significant difference in the frequency and width. However, there is a significant difference in the line-shape of G^- band for metallic and semiconducting SWNTs. G^- band appears as a Lorentzian for semiconducting tube whereas it appears as a Breit-Winger-Fano (BWF) line-shape in metallic SWNTs.[80-82]

2.1.3.1.3.3. The Disorder Induced D-Mode (D-band)

The presence of disorder in sp^2 hybridized carbon system is represented by D-band in resonance Raman spectra, located in the range of 1250-1450 cm^{-1}. This band is one of the most sensitive and informative techniques for characterizing structural defects in CNTs. The ratio of intensity between D-band and G-band typically describes the degree of damage in SWNTs during processing of the sample.

2.1.3.1.3.4. Dispersive G' Mode (G' - band)

All sp^2 carbon materials exhibit a strong Raman feature in the range 2500-2800 cm^{-1}. Together with G band, this feature is a Raman signature of graphitic sp^2 materials and is called G' band. This band is a second-order, two-phonon process that exhibits a strong frequency dependence on the excitation laser energy.

2.1.4. Dispersion of Single-Walled Carbon Nanotubes

As-produced SWNTs exist in highly aggregated states because of strong van der Waals interactions, with a pairwise binding energy of about 900 meV/nm.[83] These aggregates typically consist of aligned SWNT ropes or bundles with a hexagonal crystal-like cross-section, 20-30 nm in diameter and a few micrometers long. These SWNT ropes are usually entangled in the solid state, forming complex networks. The high binding-energy and large per-tube surface area make the SWNTs very difficult to disperse in any media.[84-87] There have been a number of attempts to develop effective methods to debundle and discretely disperse the SWNTs, including covalent and non-covalent functionalization of the SWNTs. Sonication and high shear mixing are frequently used to mechanically separate the tubes as an aid to dispersion.

2.1.4.1. Covalent Functionalization of Single-Walled Carbon Nanotubes

Covalent functionalization of SWNTs can enhance their solubility and compatibility in various polymer matrices.[88-90] These methods are based on surface or endcap functionalization of the nanotubes to improve chemical compatibility with the target medium, as well as to disrupt the smooth tube-tube interactions that are characteristic of pristine nanotubes. These processes enhance the wetting or adhesion characteristics of nanotubes and reduce their tendency to agglomerate. However, enhanced dispersion of

SWNTs in solvent or matrix system based on chemical modification, particularly along the sidewalls, can be considered a destructive approach because it deteriorates the intrinsic properties of SWNTs. Sidewall chemical modification of SWNTs involves a covalent addition reaction or oxidation. In covalent addition reactions, functional groups are directly covalently attached to the graphitic surface of SWNTs.[91,92] Some examples include fluorination,[93] derivatization with diazonium salt,[94] attachment of substituted aryl group,[95,96] and electrophilic addition of chloroform on the SWNTs surface.[97] The oxidative method involves the introduction of carboxylic acid group on SWNTs surface and followed by derivatization. Normally a mixture of HNO_3/H_2SO_4 has been used to oxidize SWNTs although other oxidative systems also work.[45] This carboxylic acid group is then converted into desired functional group.[98,99] In the method most directly comparable to the present work, polymers have been grafted on to oxidized SWNTs for incorporation into polymer composites.[100,101] These chemically modified SWNTs can be soluble in common solvents such as THF, DMF, CH_2Cl_2, CS_2, and NMP, depending on the nature of the added functional groups. [99 ,102,103]

2.1.4.2. Non-Covalent Functionalization of Single-Walled Carbon Nanotubes

Non-covalent modification of carbon nanotubes is particularly attractive because various groups can be adsorbed to the carbon nanotube surface without destroying the π system of the graphene sheets, thereby preserving the intrinsic properties of SWNTs to the greatest extent possible.[104-106] The procedures used in the literature have all been straightforward, typically involving only ultra-sonication and centrifugation or filtration. Non-covalent approaches are based on hydrophobic interactions between adsorbed molecules and the carbon nanotubes, and/or through π-π interactions (π-π stacking), and

aqueous solubility is provided by the hydrophilic part of the adsorbed molecules. Sometimes electrostatic interactions also exist between carbon nanotube and ionic adsorbents. Multiple types of surfactants and polymers have widely been used for non-covalent functionalization of SWNTs to disperse them in both aqueous and organic solutions.

2.1.4.2.1. Surfactant Assisted Dispersion

Surfactants are amphiphilic molecules that contain both a hydrophilic head group and a hydrophobic tail group. Surfactants act as solubilizers to disperse carbon nanotube in aqueous solution via physical adsorption.[87,107] The procedure of surfactant-assisted dispersion typically involves the ultra-sonication of SWNTs in an aqueous solution of surfactant. However, prolonged sonication introduces a considerable amount of defects, including buckling, bending and dislocations in the carbon nanotube structure.[108] Some of the common surfactants used for the dispersion of SWNTs are sodium dodecyl sulfate (SDS), sodium dodecylsulfonate, sodium dodecylbenzene sulfonate (SDBS), the pluronic series, triton X-100, cetyltrimethylammonium bromide, dodecyltrimethylammonium bromide, and tween 20. Among these SDS is the most widely used. Smalley, *et al*., reported the preparation of individually dispersed SWNTs by simple sonication in SDS.[41] Weisman, *et al*., demonstrated that SWNTs so-dispersed exhibited strong photoluminescence spectra in the near-IR region, proving the individuality of the tubes in such a dispersion.[75] Smalley and coworkers also studied a series of cationic, anionic, and non-ionic surfactant for their ability to disperse SWNTs in aqueous solution.[107] They found that the size of the polar head group of non-ionic surfactants was a main factor in successfully suspending SWNTs. Among the ionic surfactants, they found SDBS to be

most efficient for the dispersion of SWNTs. It has been reported that the strong interaction between SDBS and SWNTs is the combined effects of the relatively long hydrophobic chain of SDBS and the π-π interactions between aromatic moieties on the surface molecules and the graphitic surface of the nanotubes.[107] Analysis of the adsorption isotherms of SDBS on SWNTs indicates that the interactions between the surfactant molecules and the nanotube walls are mostly hydrophobic in nature. Matarredona, *et al*., discovered that carbon nanotubes can exhibit either positive or negative charges on their surfaces depending on the pH of the solution.[109] Only at pH values far from the point of zero charge do the coulombic interactions between the negatively charged head groups of the surfactant and the charged surface of the nanotubes becomes important. They also claimed that sonication time plays a key role for the dispersion of SWNTs. Santro, *et al*., explained that the surfactants adsorb and diffuse in between the unzipped gaps of the nanotubes during sonication and eventually separate the individual nanotubes from the bundle.[110] This process depends on the surfactant concentration because nanotube suspension is unstable below the critical micelle concentration of surfactant.

2.1.4.2.2. Polymer Assisted Dispersion

The dispersion of SWNTs in a surfactant is not always the best choice for the preparation of polymeric composites of SWNTs because the surfactant is very difficult to remove completely, resulting in adverse effects on the properties of the resulting polymer/SWNTs composites. Therefore, from an applications point of view, polymer-assisted dispersion is often a preferred choice. Polymer coating reduces the entropic penalty of micelle formation, and doesn't require a significant concentration of free

surfactant in the surrounding solution. However, in the case of carbon nanotubes, where hydrophobic interactions may dominate the adsorption, the use of polymers seems to give no significant improvement in dispersion efficiency as compared to surfactants.[107] There are two common methods of polymer assisted dispersion of SWNTs: polymer adsorption and polymer wrapping.

2.1.4.2.2.1. Polymer Adsorption

Polymer adsorption is based on the stacking of aromatic ring system of the polymer on carbon nanotube surface through π-π interaction, exfoliating bundles and bringing individual tubes into solution. This effect has been most effective in molecules having large aromatic systems such as pyrene.[111-114] The interaction of the aromatic systems of pyrene is so effective that functionalized pyrenes have been used for anchoring proteins and small biomolecules to the nanotubes.[115] Anthracenes are another class of polyaromatic molecules which have π-π interaction with nanotubes.[116] Murakami and coworkers have also reported porphyrin functionalized SWNTs in organic solution.[117]

2.1.4.2.2.2. Polymer Wrapping

O'Connell, *et al.*, introduced a new phenomenon called "polymer wrapping" on carbon nanotube for the reversible water-solubilization of SWNTs.[118] SWNTs have been successfully solubilized in water by wrapping with a variety of linear polymers such as polyvinyl pyrrolidone (PVP) and polystyrene sulfonate (PSS). An SDS-stabilized SWNTs dispersion was used as a starting material. The procedure was rather straightforward, with simple mixing, incubation, filtration, and centrifugation. It was proposed that the physical length of high molecular weight linear polymers and the 1D structure of nanotubes provide a wrapping scheme for hydrophobic interactions between

polymers and nanotubes. The wrapping of SWNTs by water soluble polymers is a general phenomenon, driven largely by a thermodynamic drive to eliminate the hydrophobic interface between the nanotubes and their aqueous medium. Polymers wrapped around SWNTs are typically NMR-silent, however NMR signals can be recovered upon the addition of organic solvent such as tetrahydrofuran (THF). This suggested that polymer wrapping is a reversible process, stabilized by the hydrophobic effect, and polymer nanotube interaction can be reversed by changing solvent system.

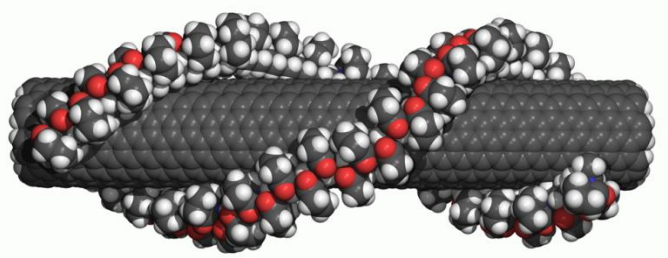

Figure 2.2. Possible polymer wrapping arrangement of PVP on SWNTs.[118]

Conjugated luminescent poly(metaphenylenevinylene) and its derivatives have also been successfully used for wrapping around SWNTs.[119] Ming Zheng and coworkers reported helical wrapping on carbon nanotube by single stranded DNA.[120] Zorbas, *et al*., demonstrated the preparation and characterization of individual peptide-wrapped single-walled carbon nanotubes.[121] These authors isolate individual peptide-wrapped SWNTs, possibly connected end to end into long fibrillar structures, using an amphiphilic α-helical peptide. Recent advances in the supramolecular assembly of biomolecules such as proteins, peptides, and nucleic acids on the surface of carbon nanotubes show great potential for applications in bioengineering.[122] Starched-wrapped SWNTs have been successfully prepared by the dispersion of SWNTs into an aqueous solution of

starch/iodine complex by mild ultasonication.[123] Similar polymer wrapping phenomena have been observed when amylose and gum arabic were used to disperse SWNTs in aqueous media.[124-126]

2.1.4.3. Challenges for the Dispersion of SWNTs

Among the most general approaches for solubilizing SWNTs is wrapping them with linear water-soluble polymer chains. Given that this approach derives its thermodynamic driving force from the hydrophobic effect, it is not surprising that a change in solvent system tends to remove the polymer wrapping from the tubes.[118] Since water is not often a solvent-of-choice for polymer processing, this general approach has seen very little development as a useful processing method for CNT composite materials. Thus, before exploring the potential application of CNTs that have been solubilized by this method, we must be able to disperse them and stabilize them in alternate solvent systems. In the present work, we explored a method for dispersing SWNTs by wrapping them individually with a crosslinkable polymer. The crosslinking of these polymer chains along each tube before removing the SWNT/polymer complexes from their initial water environment stabilizes the complexes to the point that they remain intact and individually suspendable even upon changing the solvent system.

2.2. Polyhedral Oligomeric Silsesquioxanes (POSS)

The name silsesquioxane comes from the roots “sesqui” and “ane”. “Sesqui” means one and half, indicating that a silsesquioxane molecule has a 3:2 ratio of silicon atoms to oxygen atoms. The suffix “ane” represents the hydrocarbon group. Thus, the term silsesquioxane refers to all structures which have the empirical formula $RSiO_{1.5}$,

where R is hydrogen, a hydrocarbon, or an organofunctional derivative of hydrocarbons.

Oligomeric silsesquioxane has general formula $(RSiO_{1.5})_n$. The term polyhedral indicates that the oligomers form a cage or polyhedron structure at the core of the nanoparticle. POSS are excellent example of zero dimensional nanophases where all dimensions are in the nanometer range. Oligomeric organosilsesquioxanes were first synthesized by Scott in 1946 through thermolysis of the polymeric products obtained from methyltrichlorosilane and dimethylchlorosilane cohydrolysis.[127]

Silsesquioxanes exists in various structures, including random, ladder, cage, and partial cage structures.[128] Among these structures, the cage and partial cage structures are considered polyhedral, and thus belong to the group of molecules known as POSS. These structures consist of an interior inorganic core made of silicon and oxygen and multiple organic functional groups attached to the corners of the inner-silica structure.[129,130] Because of the presence of both organic and inorganic groups, POSS are low density, high performance hybrid materials. Individual POSS particles, approximately 1-2 nm size, are often easy to disperse. Due to their small size, rigid inorganic core, and polymer-compatible organic groups, POSS are excellent candidates for the preparation of nanocomposites.

2.2.1. Synthesis of Polyhedral Oligomeric Silsesquioxanes

There are two major approaches to synthesize POSS that differ in the nature of starting materials used.[127,131-133] The first approach includes the formation of new Si-O-Si bond with subsequent assembly of polyhedral cage framework. In this method polyhedral silsesquioxanes are synthesized from monomers of the $XSiY_3$ type where X is a

chemically stable substituent (such as CH_3, phenyl, vinyl) and Y is a highly reactive substituents (such as Cl, OH, OR).

$$nXiSiY_3 + 1.5nH_2O \rightarrow (XSiO_{1.5})_n + 3nHY$$

The second approach involves the attachment of the organic group at the silicon atom without affecting interior inorganic core framework. Hybrid Plastic Co. developed a large variety of POSS by attaching different kinds of organic substituents to the silicon oxygen cage by this method.

2.2.1.1. Synthesis of Monofunctional Polyhedral Oligomeric Silsesquioxanes

Monofunctional POSS molecules can be synthesized by the controlled hydrolysis and condensation of commercially available organotrichlorosilanes.[127] The product mixture varies with reaction condition and time. Incompletly-condensed silsesquioxanes are the major products from the reaction. For example the controlled hydrolysis/condensation of cyclohexyl-trichlorosilane consists of 45% of the heptameric siloxane with three silanol groups, 40% of a hexamer and 15% of octameric cube silsesquioxanes.[127,134] The incompletely closed heptameric siloxane is easily separated from other products due to solubility differences. Then these silanol groups of the heptamer can be used to form fully a condensed POSS structure by reaction with organosilicon monomers having a reactive functional group such as triethoxysilane R-$Si(OEt)_3$. Multiple types of reactive groups can be attached using this method, including hydride, chloride, hydroxide, nitriles, amines, isocyanates, acrylics, epoxides, norbonyls, alcohols and acids.[135-138]

2.2.1.2. Synthesis of Multifunctional Polyhedral Oligomeric Silsesquioxanes

Multifunctional POSS derivatives are synthesized by hydrolysis and condensation of trialkoxysilane having reactive functional group ($R\text{-}Si(OEt)_3$). This reaction can generate octa-functional POSS, $R_8(SiO_{1.5})_{8.}$[139] A typical example is the synthesis of octaallylsilsesquioxanes from allyltrimethoxysilane.[140]

2.2.2. Hybrid Properties of Polyhedral Oligomeric Silsesquioxanes

In a POSS molecule, each silicon atom is bonded with three oxygen atoms and one hydrogen or organic group. This combination of organic and inorganic components in one molecule gives POSS its unique hybrid properties.[141] The organic substituents of POSS provide compatibility and reactivity with the polymer matrix whereas the inorganic cage provides rigidity and stability in the matrix. The major distinguishing characteristic of POSS, as compared to other nanofillers, is its versatility. The interior structure of POSS molecules closely resembles the structure of silica. Like silica and ceramic particles, the use of POSS molecules as a nanofiller can enhance the performance properties composite materials. The organic substituents of the POSS can be varied endlessly to give a range of non-reactive and reactive POSS molecules. The organic functional groups on such POSS molecules can be synthetically modified standard organic chemistry.[142]

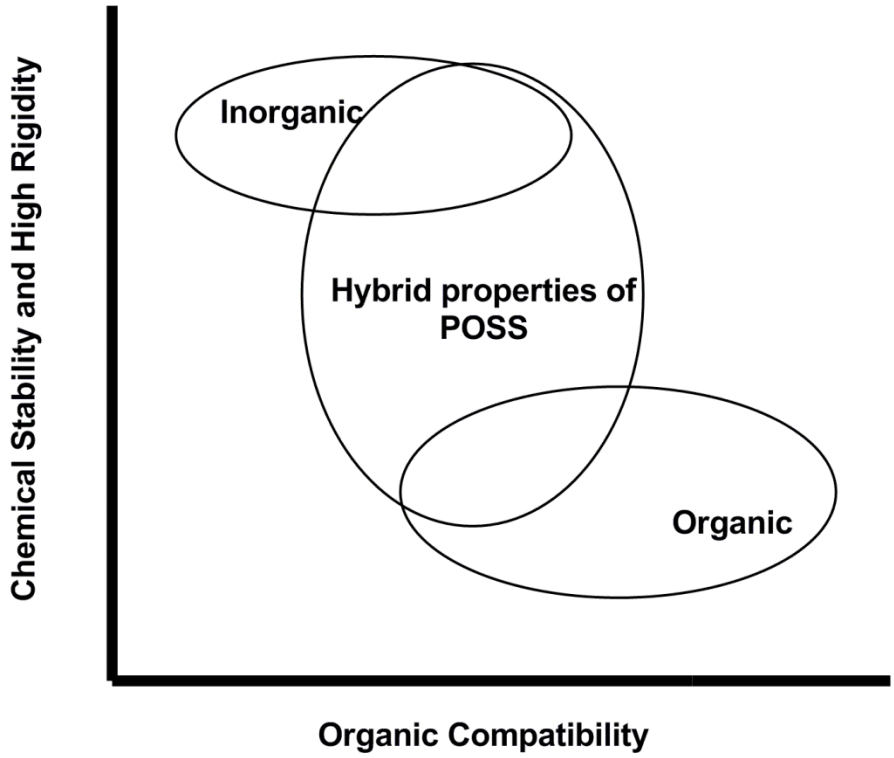

Figure 2.3. Hybrid properties of POSS.

2.2.3. Polyhedral Oligomeric Silsesquioxanes in Nanocomposites

Polymer composites are multi-constituents materials that are prepared by mixing a polymer matrix with inorganic fillers such as reinforcing fibers or particulate solids. In polymer nanocomposites, the size of the inorganic fillers is often smaller than 100 nm. The fillers, which come in a wide variety of shapes such as fibers, platelets, or spheres, are physically dispersed into polymer matrix. Such nanofillers have been shown to produce dramatic improvements in such properties as gas barrier, viscoelastic, electrical, and mechanical properties.[143-147] This property enhancement is strongly affected by the quality and nature of dispersion of the nanofillers in the polymer matrix. However, the surface energy of a material substantially increases as the particle size decreases,

resulting in an increased tendency for aggregation, naturally creating a pervasive manufacturing challenge. To avoid this problem, nanoparticles are often modified with organic groups, or coated with polymers that are compatible with the polymer matrix.[146]

POSS is available with a wide variety of organic functional groups, such as methacrylate, acrylate, styrene, norbornene, amine, epoxy, alcohol, and phenol that can render the filler compatible with the polymer matrix, allowing it to disperse well and incorporate directly into the matrix through polymerization or grafting.[135,147-150] POSS is similar to other highly symmetric molecules that can interact favorably with the polymer host in all three dimensions. The hybrid architecture of POSS makes it more compatible than purely inorganic fillers with organic hosts, such as polymers and natural biomaterials. The incorporation of POSS into a polymer matrix can modify the interactions between the molecules, local molecular topology, and polymer chain and segment mobility; as a result there is a dramatic improvement in polymer properties including improve in glass transition temperature, reduction in gas permeability, reduction in flammability and enhancement in ultimate mechanical properties.[151,152]

POSS derivatives have been extensively used to modify both thermoplastic and thermosetting polymers. Some of the recent attempts at preparing POSS-containing nanocomposites include polypropylene/POSS, polystyrene/POSS, polyester/POSS, polyamides/POSS, polyimide/POSS, polyurethane/POSS, epoxy/POSS, and polybenzoxazine/POSS nanocomposites.[151] These POSS-containing nanocomposites shows great promises for the application in light emitting diodes,[153-155] liquid crystals,[156-158] photoresist materials,[159,160] low-dielectric constant materials,[161-163] self-assembled block copolymers,[164-166] and nanoparticles.[167-169]

2.2.4. Polyhedral Oligomeric Silsesquioxanes in Epoxy Nanocomposites

Molecules with two or more α-, or 1, 2-, epoxides groups are among the most commonly-used monomers for thermosetting polymers. Such compounds are called epoxy resins. They have been used for numerous applications from surface coatings to high-performance polymers because of their excellent engineering performance upon curing. There are many advantages of epoxy resins over other thermosetting resins, including a simpler curing reaction, low shrinkage due to the absence of byproducts and volatiles during curing, and a wide range of available curing temperatures depending upon the curing agent used. The cured products of epoxy resins are versatile and exhibit superior properties such as excellent chemical and heat resistance, excellent fatigue resistance, high tensile strength, low creep, high adhesive properties, high electrical insulation, and an excellent ability to withstand degradation from water ingress.

However, the inherent toughness of the cured products is relatively low due to their high crosslink densities. As a result, they are brittle and do not resist the crack initiation and growth well. These problems of epoxy resins limit their performance in the applications that require high impact and fracture strengths. It is therefore desirable to modify the epoxy resins to enhance these properties. In recent years considerable attention has been given to POSS as a modifier or nanofiller to enhance these key properties of epoxy resins.

It has been reported that the nanoscopic size of the POSS cage has ability to hinder the segmental motion of molecular chains and network junctions within an epoxy composite, resulting in an increase in the glass transition temperature.[146,170-173] Kim, *et al.*, prepared an octaglycidyl dimethylsilyl-POSS (OG-POSS) and cured with 4’4’-

diaminophenyl sulfone (DDS) to study the toughening mechanism of the resin.[174] Thermal analysis showed that both glass transition temperature and storage modulus increased with increasing the concentration of DDS due to an increase in crosslinking density. The toughening mechanism of the resin was found to be void formation. Another study by Liu, *et al*., reported that the glass transition temperature remained unchanged at OG-POSS loading < 30 wt.%, whereas the nanocomposites displayed lower T_g at OG-POSS concentration greater than 40 wt.%.[140] Xiao *et al*. found that the curing reactions of POSS composites are more difficult than neat epoxy resin because of increased steric hindrance.[175] They demonstrated that high crosslinking through eight vertices of the POSS core froze the motion of main polymer chain, resulting in a POSS composite material that did not exhibit obvious glass transition behavior.

Zhang and coworkers demonstrated the enhancement of viscoelastic and mechanical properties of epoxy resins with the addition of POSS-NH_2 monomer.[176] They found excellent results in the lower content of POSS macromers. Lee, *et al*., investigated enhancement in thermal and viscoelastic properties of epoxy resin with the incorporation of monofunctional epoxy-POSS macromers.[170] In this system, the T_g was observed to increase and broaden with increasing weight fraction of epoxy-POSS content because of the influence of POSS cage to the polymer chain motion. In another study, significant enhancement was found in flexural and thermal properties of the epoxy composite material with the addition of 1 or 2 vol. % of POSS content.[170]

CHAPTER 3

EXPERIMENTAL SECTION

This chapter describes the experimental methods and materials used in this study. The detailed instrumentation and experimental procedure are explained in this chapter.

3.1. Materials

Purified HiPco single-walled carbon nanotubes were obtained from Carbon Nanotechnologies Inc. Sodium dodecyl sulfate (SDS), poly(diallyldimethylammoniumchloride) (PDDA), 2,2′-azobis(2-methylpropionitrile) (AIBN), isophorone diamine (IPDA) were obtained from Sigma-Aldrich. Allylamine (AAm) and N-vinylpyrrolidone (VP) were obtained from Acros Organics Polysciences Inc. EPON 862 and glycidyl -POSS cage mixture (oxirane, 2-[[3-(trimethoxysilyl)propoxy]methyl]-, hydrolyzed) were obtained from Hexion Specialty Chemicals, Inc. and Hybrid Plastics respectively. Nanopure distilled water was produced by Direct-Q UV-3 distillation system (Millipore). Dialysis sacks MWCO 3500 and MWCO 20000 were obtained from Thermo Scientific.

3.2. Instrumentation

3.2.1. Ultrasonication, High Shear Mixing and Centrifugation

Ultrasonic dispersion of SWNTs was performed using a FS-140H ultrasonic bath with 135 W power output and a GEX-750-5C ultrasonic processor (Sonics & Materials Inc.) equipped with a tapered tip at 10 – 20 W power. High shear mixing was performed using an Ultra-Turrax T18 mixer (Ika Werke GMBH). Low speed centrifugation was performed on a Sorvall Biofuge Stratos centrifuge and high speed centrifugation was done on a Beckman L8-70M ultracentrifuge using a Ti75 rotor.

3.2.2. Fluorescence Spectroscopy

Fluorescence spectra of the SWNTs dispersions were acquired on a NS-1 Nanospectralizer (Applied Nanofluorescence, Inc.) using 678 nm and 782 nm excitation lasers with aqueous 1% SDS solution as the background. 500 μL of aqueous suspended SWNTs were placed into the NanoSpectralyzer's sample cell (Starna Cells, Inc. part 9F-SOG-10-GL14-C) with path lengths of 10 mm in one direction and 4 mm in the perpendicular direction. Photoluminescence was detected at 90^{o} by a 512 element InGaAs array.

3.2.3. Absorption Spectroscopy

The absorption spectra of the SWNTs dispersions were taken by using a CARY-5000 spectrophotometer with aqueous 1% SDS solution as the background. The measurements were carried out in 1 cm path-length quartz cells in the range of 175-1500 nm.

3.2.4. Atomic Force Microscopy

Atomic force micrographs were taken on a Multimode Nanoscope IIIa SPM (Digital Instruments) equipped with NSC 15/50 silicon cantilevers (MikroMasch) in tapping mode. For the samples preparation, a mica chip was first primed by applying a drop of 10% aqueous PDDA solution to the chip for 10 min followed by quick rinsing with water and drying in a nitrogen flow. A drop of the SWNTs dispersion was applied on the primed surface for 30 min. The liquid was sucked from the chip with a pipette; the chip was then rinsed with ethanol for 1-2 s and dried in a nitrogen flow.

3.2.5. Raman Spectroscopy

Raman spectra of epoxy/POSS composite materials were recorded in a WITec alpha300 R Raman instrument with 532 nm laser excitation at a power of 15 mW with a 20 micron spot size.

3.2.6. Dynamic Mechanical Analysis (DMA)

The storage modulus (E'), loss modulus (E''), and tan delta were determined by DMA analysis of each samples of the composite materials. DMA was performed on a DMA Q800 instrument (TA Instrument Company, USA) at a frequency of 3 Hz from 25 ^{o}C to 250 ^{o}C at a ramping rate of 3 ^{o}C/min. For each group, five replicates with a sample size of 60 x 12 x 1 mm were tested.

3.2.7. Differential Scanning Calorimetry (DSC)

DSC were recorded on a DSC Q2000 (TA Instrument Company, USA) in a dry nitrogen atmosphere. The instrument was calibrated with an indium standard. Approximately 8 mg of sample was heated from room temperature to 200 ^{o}C at a ramp rate of 10 ^{o}C/min in a DSC cell. The sample was cooled immediately to 0 ^{o}C at the same

scan rate. A second scan was then performed under the same conditions. The reported data were extracted from second scan. A minimum of five replicate samples were analyzed for each sample type.

3.2.8. Fracture Toughness Measurement

Fracture toughness of the sample was measured on a universal testing machine (Instron 5567, Norwood, MA). The measurement was carried out by using the single-edge notch bend test as per the ASTMD–5045 standard method. A 4.5 mm deep notch was made in each 54 x 12.7 x 6.35 mm samples by a diamond precision saw. To make a natural pre-crack initiation from the notch, the tip of the notch was gently tapped with a razor blade using a hammer. The tests were performed under three point bending until failure. A minimum of five samples were tested for each group. The fracture toughness was expressed in term of the critical stress intensity factor (K_{Ic}) according to following equation:

$$K_{Ic} = \frac{P}{B\sqrt{W}} f\left(\frac{a}{W}\right)$$

Where P = applied force, B = thickness of the specimen, a = crack length W = the width of the specimen and f = the geometric factor.

3.2.9. Helium Gas Permeability

The gas permeability of the samples was tested by the ASTM standard D1434-82 volumetric method. The experimental setup follows the guideline provided by NASA.[235] The apparatus consists of two chambers between which a 25.4 mm diameter, 3.15 mm thick specimen is placed. Purified helium gas was pressurized in the upstream chamber, allowed to permeate through the sample, and escaped into the downstream chamber. Two

pressure transducers (model: PX01C1-075G5T, Omega Dyne Inc.) were connected to the inlet and outlet ports to acquire precision pressures of the upstream and downstream chambers. The pressure data was obtained on an oscilloscope (Tektronix TDS 460 A). The apparatus also includes a high capacity gas purifier to remove any impurities present in the helium gas. After calibration, a minimum 5 samples from each group were tested. The permeability of the nanocomposite samples was evaluated in terms of the permeability coefficient, which is calculated by using the Darcy equation.

$$Q = \frac{K}{\eta}\frac{\Delta P}{L}A$$

Here Q = flow rate, K = permeability coefficient, ΔP = pressure difference, L = thickness of the test sample, η = dynamic viscosity of Helium, and A = cross-sectional area to flow.

3.2.10. Scanning Electron Microscopy

Fracture surface morphology was studied by Scanning Electron Microscopy (SEM). The samples were coated by sputtering Gold-Palladium using a Balzers Union MED 010 Au/Pt coater to make them conductive. SEM micrographs were taken in FEI Quanta 600 field-emission gun environmental scanning electron microscope with an Evex EDS X-ray microanalysis system and HKL EBSD system.

3.3. Procedures

3.3.1 Dispersion of Single-Walled Carbon Nanotubes in Aqueous Solution of SDS

A 1% solution of SDS in water was prepared and the pH was adjusted to 9.0 by the addition of NaOH. 2.5 mg of SWNTs were dispersed in 50 mL of the SDS solution by bath sonication for 1 hour followed by stirring for 12-15 hours. The dispersion was

subjected to high shear mixing for 1 hour at minimum speed (high speed induces excessive foaming) followed by tip sonication at 10-15 W power by 10,000 J increments (1000 J of energy = sonication at 10 W for 100 s). The fluorescence spectra were taken frequently to optimize the conditions for dispersal. Dispersed SWNTs were also analyzed by AFM.

3.3.2. Dispersion of Single-Walled Carbon Nanotubes in Water with the aid of PVP

2.5 mg of SWNTs were dispersed in 50 mL of 1% aqueous solution of SDS, pH adjusted to 9.0, by following the process described in section 3.3.1**.** The aqueous suspension of SWNTs was centrifuged at 1500 rpm to bring the large bundles of SWNTs to the bottom of the centrifuge tube. The upper 75 to 80% of the supernatant was then carefully decanted, resulting in surfactant-suspended nanotube dispersion at a typical mass concentration of 20 to 25 mg/L. Then 5 mL of 110 g/L aqueous solution of PVP was added to the SWNTs dispersion (final conc. of PVP = 10 g/L) and the mixture was incubated at room temperature for up to 20 hours. The resulting sample was vacuum filtered through a 1 μm polypropylene track-etched membrane and the filtrate was ultra-centrifuged at 200,000 g for 2 hours. The transparent supernatant was decanted, the solid redispersed in 50 mL of water, and two more cycles of ulta-centrifugation/redispersion were repeated. The final solid was redispersed in 20 mL of water by 30 min of bath sonication.

3.3.3. Synthesis of Cross-linkable Copolymers of PVP

The following cross-linkable copolymers of PVP were synthesized: poly (N-vinylpyrrolidone-co-2-aminoethyl methacrylate) (PVP-PAEMA), poly(N-vinylpyrrolidone-co-2-hydroxyethyl methacrylate) (PVP-PHEMA), poly(N-

vinylpyrrolidone-co-allylamine) (PVP-PAAm) and poly(N-vinylpyrrolidone-co-N-acryloxysuccinimide) (PVP-PNAS). Structures for the polymers are presented in Figure 3.1. All polymers were used to disperse SWNTs in aqueous suspension. PVP-PHEMA was found to be insoluble in water. PVP-PAEMA and PVP-PNAS were soluble in water but unable to disperse SWNTs in water. Only PVP-PAAm successfully achieved good results for the dispersion of SWNTs. Thus the synthesis process of PVP-PAAm is the only one described in this dissertation.

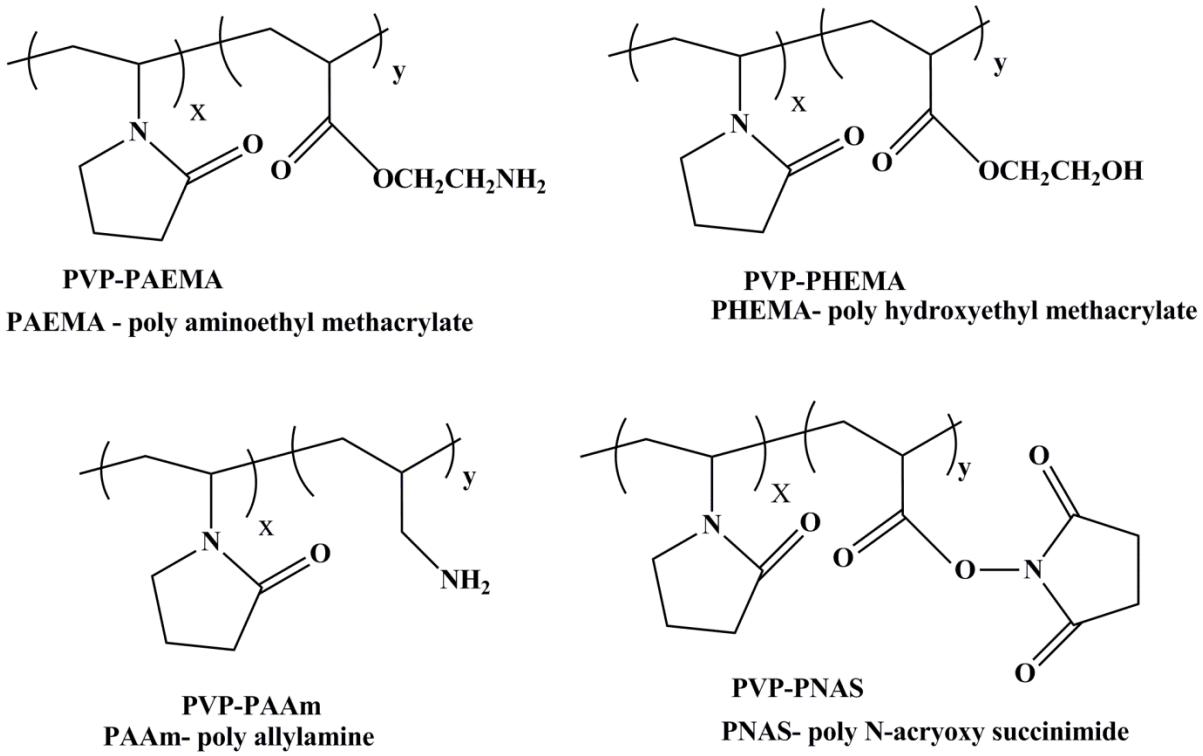

Figure 3.1. Structure of some crosslinkable copolymers of PVP.

3.3.4. Synthesis of PVP-PAAm

This random copolymer was synthesized from the method of Solovskii *et al*. by free radical polymerization of VP and AAm.[233] A mixture of 10g of VP (80 mole %), 1.29g of AAm (20 mole %) and 0.38g of AIBN (1 mole %) was dissolved in 35 mL of isopropanol. The solution was transferred into a 100 mL Schlenk flask equipped with a stir bar and degassed by 3 cycles of freeze-pump-thaw. The stopcock was closed under vacuum and the flask was immersed into an oil bath at 70 ^{o}C and stirred for 48 hours. The reaction was stopped by cooling the flask to room temperature and opening it to air. The solution was precipitated in a large amount of diethyl ether and the product was collected on a schott filter. The white solid was dissolved in 70 mL of water and the excess monomer was removed by dialysis against deionized water using a 3500 Da MWCO sack, until no monomer in the outside water was detected by UV spectrometry. The solution was concentrated on rotary evaporator at 35^{o}C until the solution had a honey-like viscosity. The remaining water was removed under vacuum (3-5 mm Hg) for 24 hours to obtain copolymer PVP-PAAm with a 7 mole % primary amine group and viscosity averaged molecular weight 15,000 g/mole.

3.3.5. Dispersion of Single-Walled Carbon Nanotubes with PVP-PAAm

5 mL of a 110 g/L aqueous solution of PVP-PAAm was added to 50 mL of the suspension of SWNTs in SDS (as described in section 3.3.1.) and the mixture was incubated at room temperature for up to 12 hours. Fluorescence spectroscopy indicated that the interaction of the SWNTs with the polymer strands was largely completed during the first 20-30 min after addition and longer incubation resulted only in re-bundling of nanotubes as measured by a loss of fluorescence signal. The resulting sample was

vacuum filtered through a 1 μm polypropylene track-etched membrane. The samples were subjected for 3 cycles of ultra-centrifugation at 200,000 g for 2 hours, decantation, and resuspension. The final solid was redispersed in 20 mL of water by 30 min of bath sonication. These three cycles of ultra-centrifugation/decanting/resuspension, modeled after the O'Connell procedure, removed the surfactants and excess of polymer.[54] As an alternate procedure that ultimately resulted in better suspensions, we subjected the sample to only one ultracentrifugation/decantation/resuspension step followed by dialysis using 20,000 Da MWCO sacks against deionized water for 72 hours. The comparison of these two methods is explained in section 4.2.1.

3.3.6. Crosslinking of PVP-PAAm

After the adsorption of polymer onto the SWNT surface, PVP-PAAm was cross-linked under dilute conditions in the aqueous environment.[233, 234] The crosslinking process was carried out by heating 10 mL of the solution with 10 μL of gluteraldehyde (GLU) at 50 ^{o}C for 8 hours in a nitrogen atmosphere. In order to avoid the crosslinking of the PVP-PAAm between different tubes, we kept the concentration of SWNTs very dilute. During this process, GLU crosslinks the amine (NH_2) groups of the polymer via an azomethine bond (N=CH).The presence of the azomethine (imine) group was confirmed in the resulting pale yellow suspension by absorption spectroscopy, since it gave two absorption peaks at 457 nm and 538 nm. Excess GLU was removed by extracting twice in 10 mL diethyl ether. After crosslinking the polymer, the stability of SWNTs dispersion was analyzed by fluorescence, absorption spectroscopy, Raman spectroscopy and AFM.

3. 3.7. Synthesis of Epoxy/POSS Nanocomposites

3.3.7.1. Selection of Epoxy Resin, Curing Agent and POSS

EPON Resin 862 was used as a composite matrix. This resin is a bifunctional epoxy resin that consists of oligomers of diglycidyl ethers of bisphenol F (DGEBF) (Fig. 3.2 a). EPON 862 was chosen for this study because of its low viscosity, superior mechanical properties, chemical resistance, and ease of fabrication. Some of the properties of EPON 862 are listed below (Table-3.1).

Table 3.1. Properties of EPON 862 *

Properties	Unites	Value
Weight per Epoxide	g/eq	165-174
Viscosity at 25 ^{o}C	P	25-45
Density at 25 ^{o}C	g/ml	0.98

*Source- Technical data sheet of EPON 862

The curing agent used was isophorone diamine (IPDA) with an equivalent molecular weight of 170.3 gm/equiv (Fig 3.2 b). IPDA is a cycloaliphatic amine, a class of molecules that is commonly used as curing agents for epoxy resins, providing lower viscosity and better chemical resistance than other curing agents.

The POSS molecule used in this work was a glycidyl-POSS cage mixture (Fig. 3.2 c). Glycidyl-POSS is a multifunctional POSS epoxide that, due to its epoxide groups, has a high compatibility with common epoxy resins, and can covalently crosslink directly into the resulting composite matrix. Glycidyl-POSS is a potential candidate for vacuum-

assisted resin transfer molding (VARTM) of fiber reinforced composites because of its low viscosity at room temperature. Some of the properties of glycidyl-POSS cage mixture are listed below (Table-3.2).

Table 3.2. Properties of glycidyl POSS cage mixture*

Properties	Unites	Value
Weight per Epoxide	g/eq	167
Viscosity at 25^{o}C	P	48
Density	g/ml	1.25

*Source- Technical data sheet of glycidyl POSS cage mixture from Hybrid Plastic

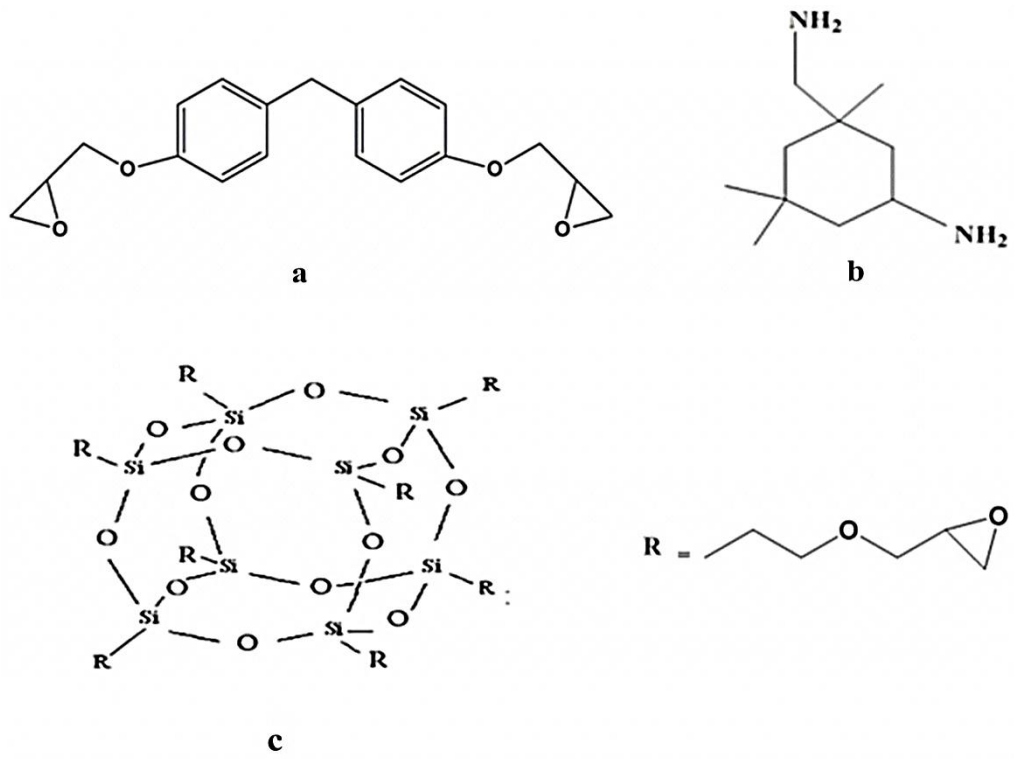

Figure 3.2. Structure of DGEBF (a), IPDA (b) and Glycidyl POSS (c).

3.3.7.2. Specimen Preparation for Epoxy /POSS Nanocomposites

Glycidyl-POSS was mixed in varied proportions of 0, 0.25, 0.5, 1, 2, 3 and 5 wt. % into the Epon 862 resin. The mixture was stirred continuously with a stir bar in a vial for 2 hours at 65 ^{o}C. After the mixture was cooled to room temperature, a stoichiometric amount of IPDA with respect to Epon 862 resin (4 parts Epon 862 to 1 parts IPDA by mass) was added with continuous stirring until the complete homogenous dissolution of curing agent was attained. Homogeneity of the mixture was observed visually. The mixture was then placed in a vacuum chamber for 30 minutes for degassing in order to remove gas bubbles that were introduced during mixing. The mixture was poured into a Teflon-coated mold and cured at 90 ^{o}C for 90 minutes and post-cured at 200 ^{o}C for a further 90 minutes.

CHAPTER 4

DISPERSION OF SINGLE-WALLED CARBON NANOTUBES BY ENCAPSULATION IN A LINEAR CROSSLINKABLE POLYMER

This chapter contains the result and discussion concerning the dispersion of single - walled carbon nanotubes (SWNTs) by encapsulation in a linear crosslinkable polymer. The first part of the chapter includes the study of dispersion of the SWNTs with the addition of surfactant and PVP, whereas second part of the chapter deals with the study of the stability of SWNTs dispersion after the crosslinking the polymer on the SWNTs surfaces.

4.1. Dispersion of Single-Walled Carbon Nanotubes

The objective of the research is not only to achieve the dispersion of SWNTs but also to stabilize them against changes to the solvent system. Our SWNTs dispersion approach is based on the O'Connell, *et al,*. method of polymer wrapping.[118] Using this technique we successfully prepared the SWNTs dispersion in SDS and wrapped them by adding PVP in aqueous solvent.

4.1.1. SDS Assisted Dispersion of Single-Walled Carbon Nanotubes

The dispersion of SWNTs in aqueous SDS was monitored by near-infrared fluorescence. Figure 4.1 shows how the fluorescence spectrum of the dispersion at 658

nm excitation changes based on duration of sonication. The plots show a rapid increase in the fluorescence intensity with increasing sonication energy. The highest intensity of the fluorescence was found at 140 kJ. The increasing fluorescence intensity reflects the increasing number of individual nanotubes that were split from the bundles during the sonication process.

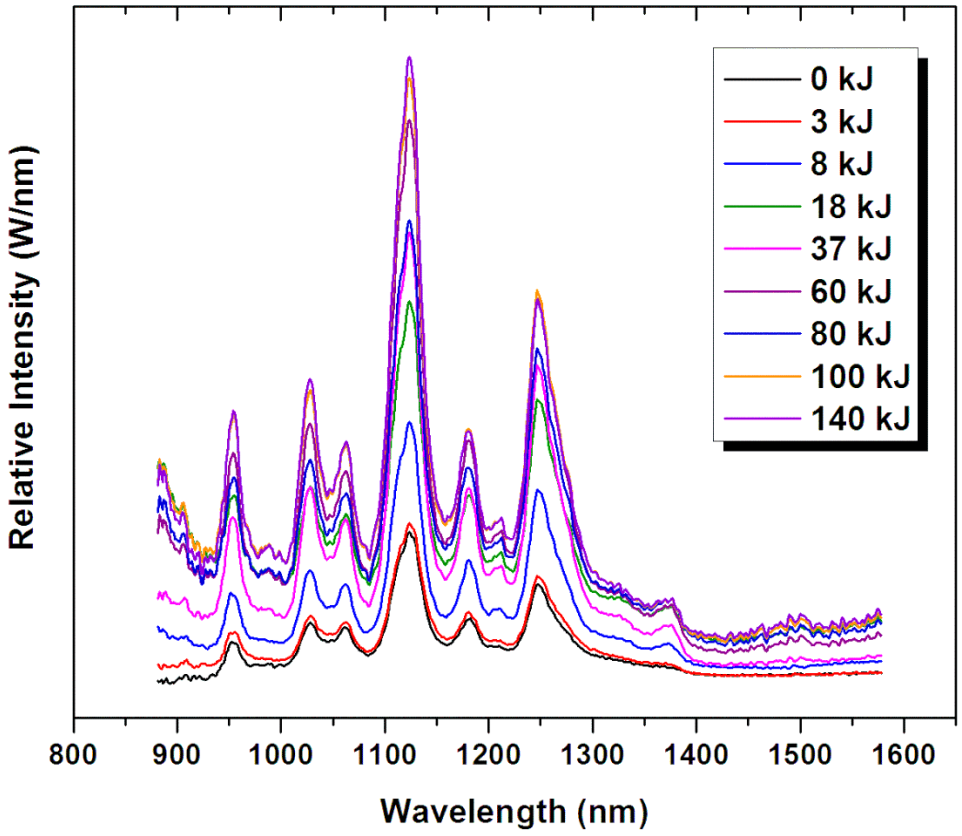

Figure 4.1. Fluorescence spectra under 658 nm laser excitation of SWNTs dispersions in aqueous SDS solution at different sonication energy.

Figure 4.2 shows the AFM micrographs of the SWNTs samples after 60 and 120 kJ of sonication, following deposition on mica as described in section 2.4.2. Height analysis revealed a noticeable reduction in bundle diameter after 60 kJ of sonication, while many of them were longer than 1 μm. The 120 kJ sample contained predominately short nanotubes < 0.5 μm. These results suggest that the best condition for dispersion SWNTs will be sonication for 60 kJ, or 100 min at 10 W of output power.

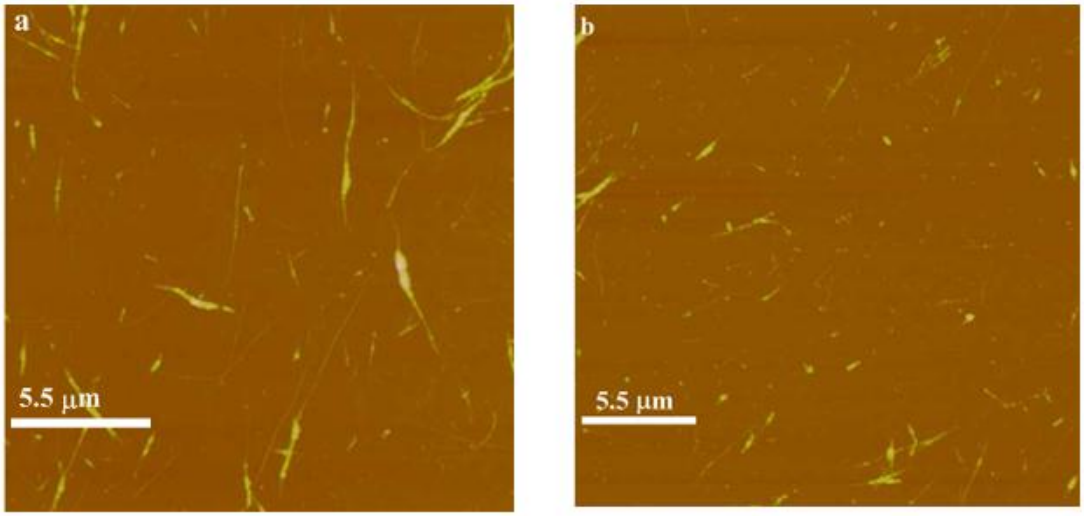

Figure 4.2. AFM images of SWNTs dispersion (a) after 60 kJ (b) 120 kJ ultrasonic energy introduced to the samples.

4.1.2. PVP Assisted Dispersion of Single-Walled Carbon Nanotubes

After the successful dispersion of SWNTs in an aqueous solution of SDS at basic pH, we added PVP to wrap the individual SWNTs. Following the procedure of O'Connell, *et al.*[118] we used the intrinsic fluorescence of the SWNTs to monitor the individualization of SWNTs (Figure 4.3).[41] Several sequential changes to the

fluorescence spectra occurred after the addition of PVP to the SWNTs dispersion. First, nearly immediately a spectral shift in the peak position with little change in intensity was observed. This change reflects a specific interaction of SWNTs with PVP molecules, producing a shift of optical transition energy (S_{ii}) due to changes in the local environment as the SDS molecules are replaced by PVP. Giordani, *et al.*, observed a similar spectral shift from SWNTs dispersed in NMP, a small molecules with cyclic amide groups similar to PVP, as comparison to water-surfactant dispersions.[236] This spectral shift might be caused by the higher dielectric constant of PVP than that of long chain hydrocarbon SDS.[237, 238] Over longer timeframes, there was a slow decrease in the peak intensity without shift that resulted from prolonged incubation after the addition of PVP. This prolonged incubation (up to 20 hours) likely allowed the rebundling of SWNTs, resulting in a decrease in the intensity of the fluorescence peaks. Finally, we observed a near-complete quenching of fluorescence after the addition of few drops of THF. The addition of even a small amount of THF reduces the surface tension of the water dramatically, and thus reduces the hydrophobic effect significantly. This removes the thermodynamic drive for the polymer to adsorb to the surface of the tubes, destroying the PVP-SWNTs complex and regenerating the initial components, where the nanotubes precipitate from suspension and lose their semiconductor fluorescence due to bundling with metallic tubes.

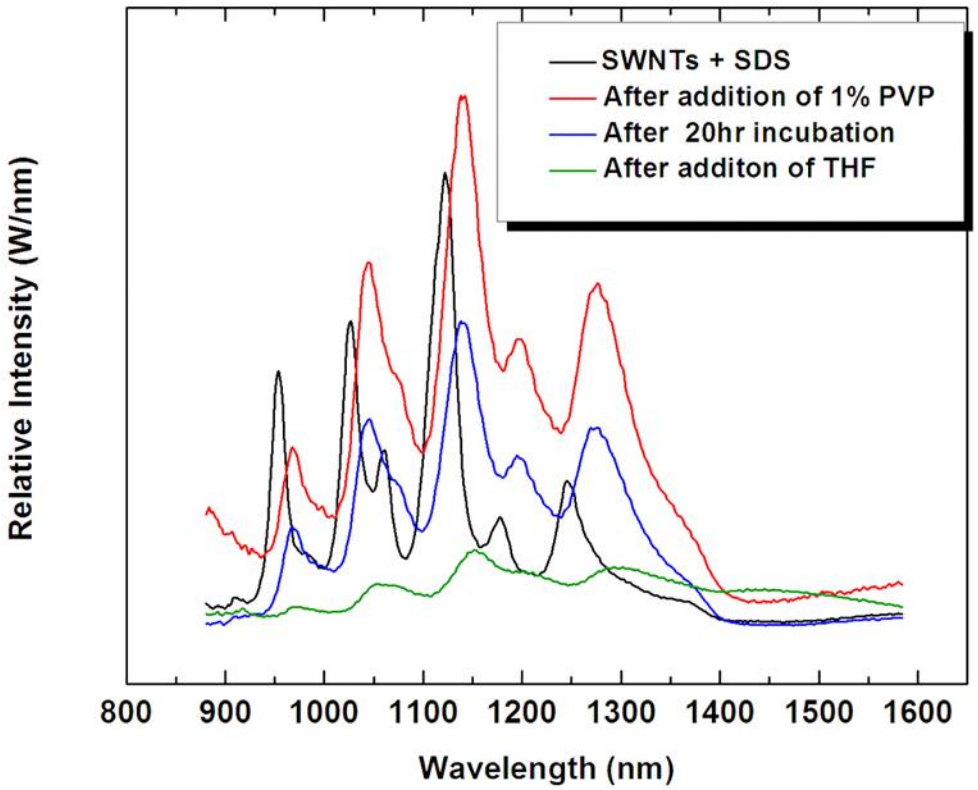

Figure 4.3. Fluorescence spectra of SWNTs dispersions at different stages of the procedure before and after the addition of PVP.

4.2. Stability of Dispersion of Single-Walled Carbon Nanotubes

The separation of PVP from the SWNTs surfaces upon changing solvents is a major hurdle to using polymer-wrapped SWNTs for composite applications. We have designed a crosslinkable polymer to use in place of PVP. Since PVP itself lacks crosslinkable groups, we synthesized PVP-PAAm, a water soluble crosslinkable copolymer of PVP. This copolymer has primary amine groups that can be easily crosslinked by gluteraldehyde (GLU).

4.2.1. PVP-PAAm Assisted Dispersion of Single-Walled Carbon Nanotubes

The initial wrapping of SWNTs with PVP-PAAm followed a similar pattern to that observed for PVP. The addition of PVP-PAAm resulted in an immediate shift in the peak positions along with the decrease in intensity and broadening of the peaks (Figure 4.4). The intensity was restored over the course of several hours. As the fluorescence spectroscopy indicated, the interaction of SWNTs with polymer was basically completed during the first 5 min after the addition of PVP-PAAm. The spectral shift of the fluorescence spectra indicates the polymer wrapping on SWNTs. As was explained above, changing in dielectric environment of SWNTs is likely responsible for the spectral shift.

The fluorescence of nanotubes after 3 cycles of high speed centrifugation decreased significantly compared to the material after filtration, even though the concentration of SWNTs in the final sample was higher than that in the filtrate. These results suggest that the nanotubes after centrifugal washing of the excess of SDS and PVP-PAAm have mostly re-bundled. This method was modified by using dialysis through a 20,000 Da MWCO sack for 72 hours in place of the last two centrifugation/decantating/resuspension cycles. The near-infrared fluorescence after dialysis confirms the presence of individual SWNTs in the solution. Figure 4.5 shows the comparison of fluorescence spectra after ultra-centrifugation and dialysis steps. As was observed for PVP-wrapped SWNTs, the fluorescence was quenched after the addition of a few drops of THF. This quenching demonstrates that changing the solvent system tends to remove the polymer from the SWNTs surface, once again bundling the tubes.

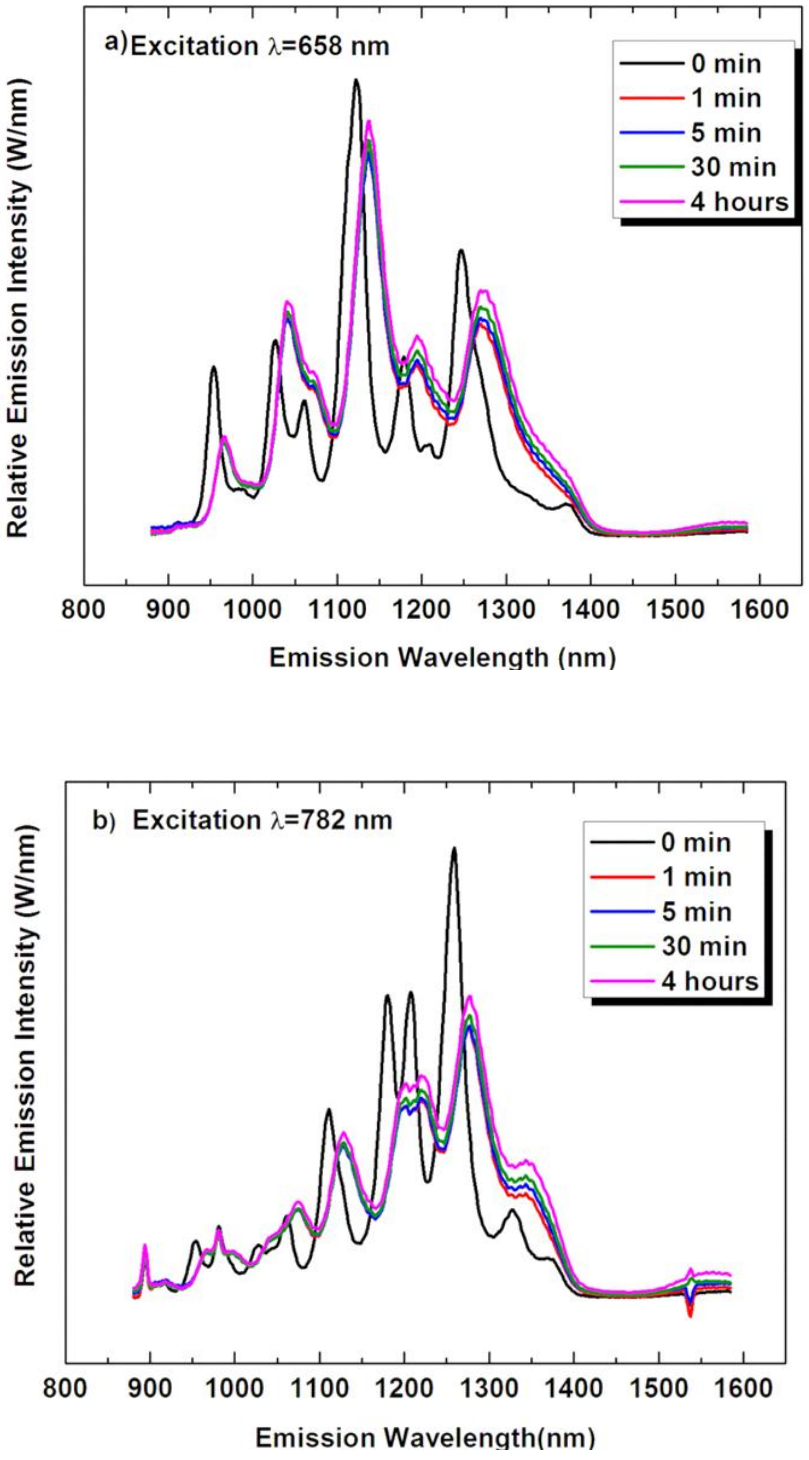

Figure 4.4. Fluorescence spectra of SWNT upon addition of PVP-PAAm at (a) 658 nm (b) 782 nm excitation wavelength.

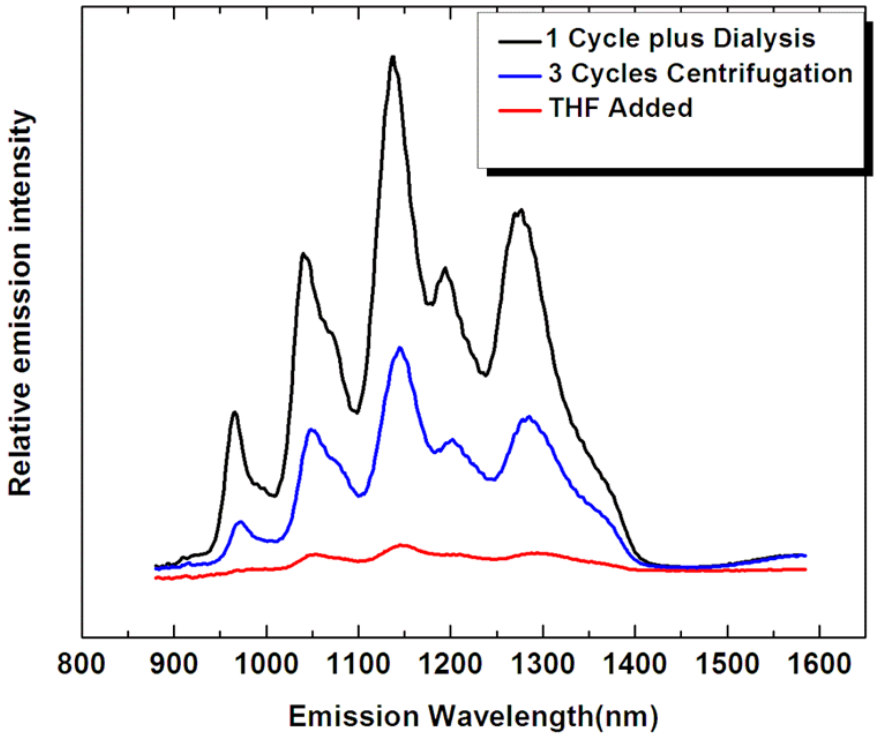

Figure 4.5. Fluorescence spectra taken at 658 nm excitation wavelengths during the removal of surfactant and excess of polymer after polymer wrapping on SWNTs.

4.2.2. Crosslinking of Polymer and Verification of Crosslinking

The polymer was crosslinked by gluteraldehyde (GLU) as described in section 3.3.6**.** During this process, GLU crosslinks the amine (NH_2) group of the polymer via azomethine bond (N=CH) (Figure 4.6). The presence of the resulting azomethine (imine) group was confirmed in the resulting pale yellow suspension by absorption spectroscopy, since it gave two absorption peaks at 457 nm and 538 nm.

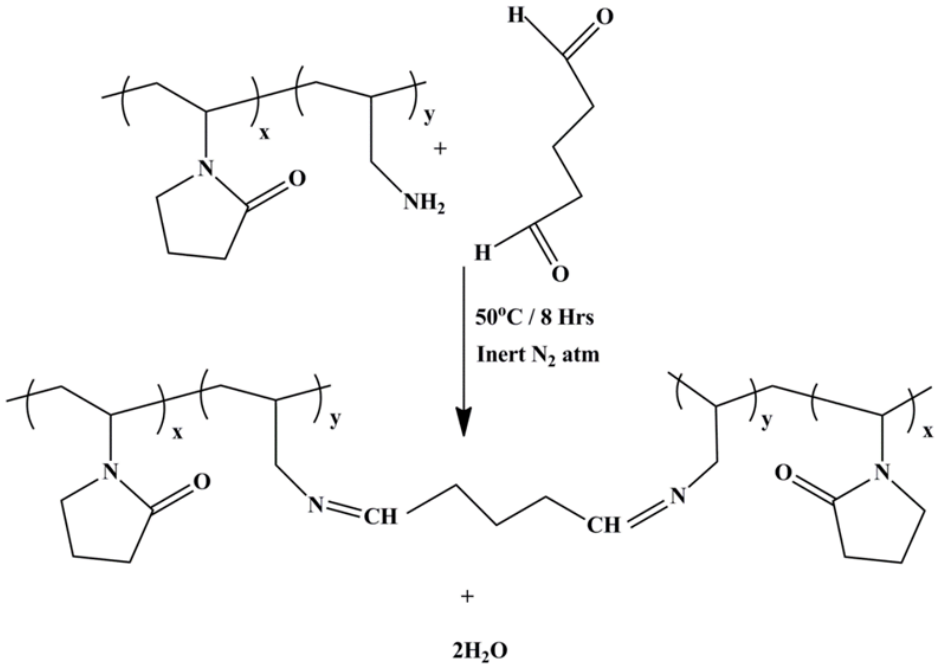

Figure 4.6. Crosslinking of PVP-PAAm by glutaraldehyde.

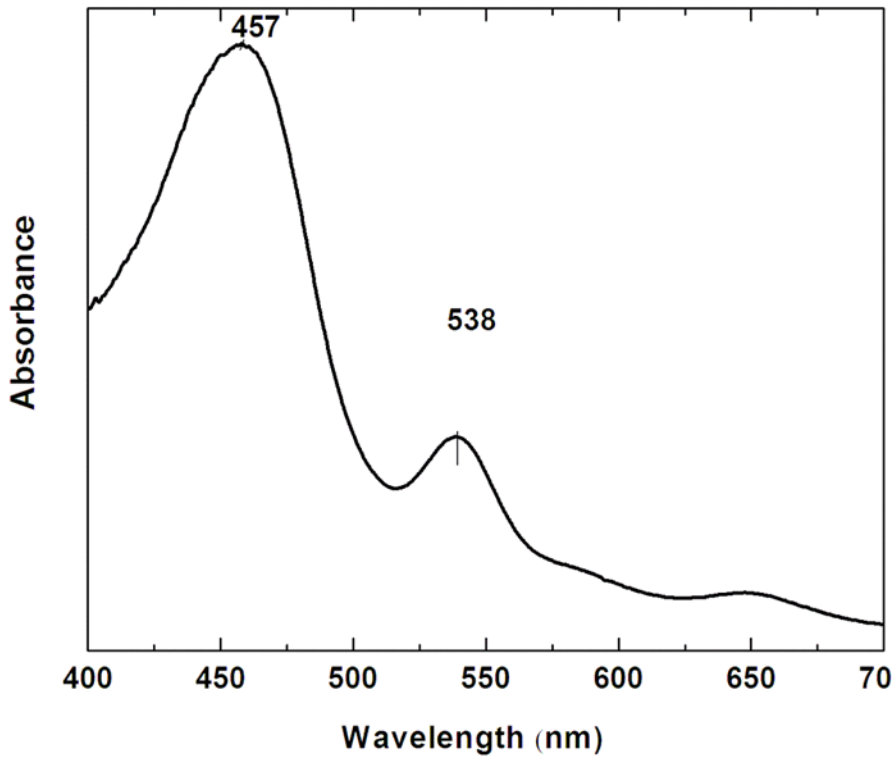

Figure 4.7. UV-Vis absorption spectra of glutaraldehyde-crosslinked polymer.

4.2.3. Stability of Single-Walled Carbon Nanotubes Dispersion after Crosslinking of PVP-PAAm

Figure 4.8 compares the fluorescence spectra taken at 658 nm excitation during the different stages of the dispersion of SWNTs. We first see a shift in the spectrum after the addition of PVP-PAAm. However, there is little significant spectral change after the crosslinking of the polymer, clearly suggesting that the crosslinking of polymer has little effect on the local electronic environment or on the quality of the dispersion. Most importantly, unlike the case of PVP or the pre-crosslinked PVP-PAAm, the fluorescence spectrum remains unchanged after the addition of THF. This observation strongly supports our conclusion that the crosslinking of the polymer prevents its removal from SWNTs. This strongly suggests that a dispersion of polymer-wrapped SWNTs can be stabilized for use in other solvent systems if they are wrapped with a polymer that has been cross-linked before removing the polymer/nanotube complex from its aqueous environment.

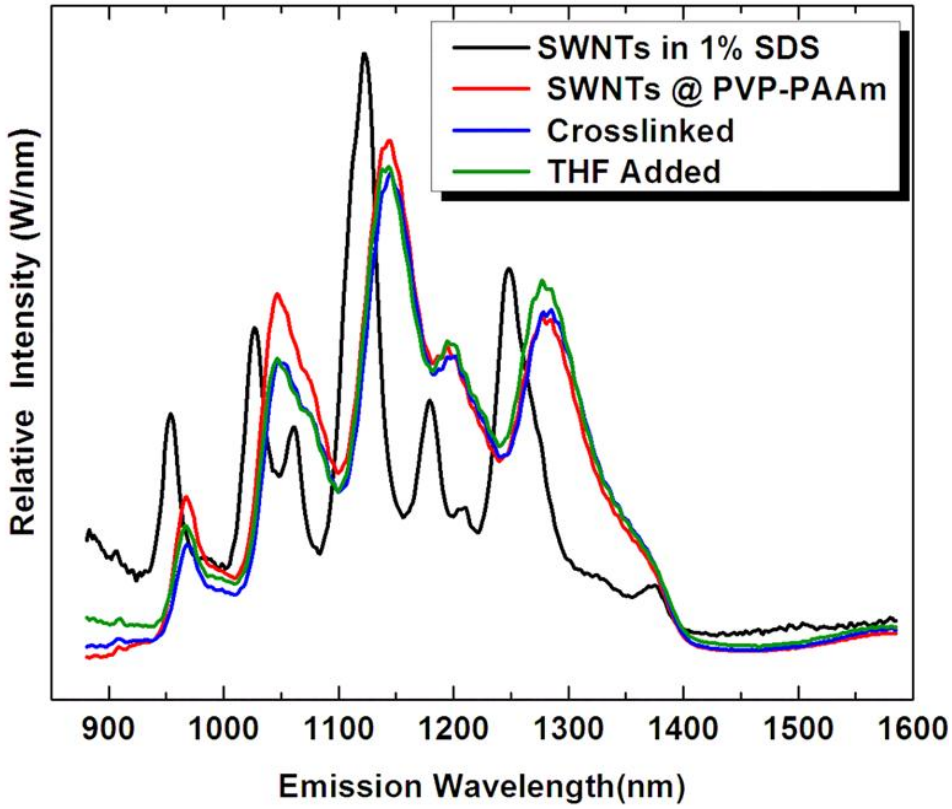

Figure 4.8. SWNT fluorescence spectra taken at 658 nm excitation while dispersed in SDS (black), after the SDS has been replaced by PVP-PAAm (red), after crosslinking with GLU (blue), and after adding THF to the suspension (green).

The dispersion of SWNTs was further characterized by vis-NIR absorbance. As is shown in Figure 4.9, all the optical transitions (E_{11}, E_{22}, M_{11}) are present in our samples, indicating that this approach does not alter the electronic properties of SWNTs.

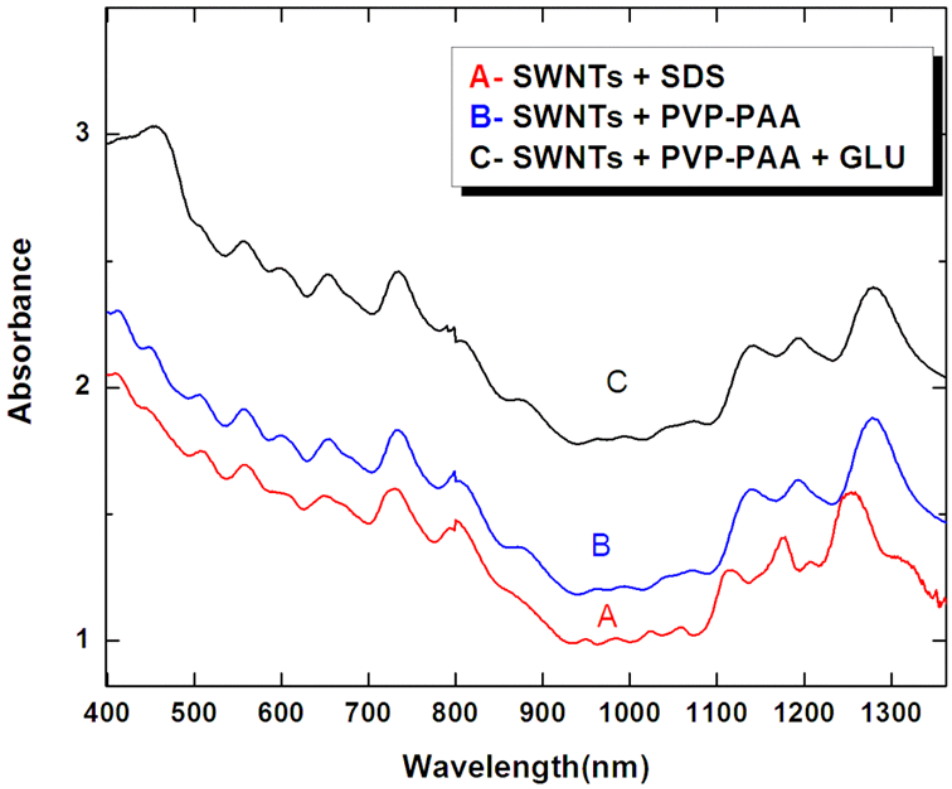

Figure 4.9. Vis-NIR absorbance of SWNTs in SDS (A), polymer wrapped SWNTs before (B) and after crosslinking (C).

AFM images of polymer wrapped SWNTs after crosslinking with GLU are shown in Figure 4.10. The height profile of such images reveals that the nanotube/polymer complexes have an average diameter ranging from 3 to 4 nm. These observed diameters are larger than that of individual HiPco SWNTs, which had an initial average diameter of 1 nm. The thickening of the nanotube can be accounted by a uniform polymer coating on each nanotube with a thickness of 1 to 1.5 nm. The AFM images confirm that the individual nanotubes are separated well so that crosslinking could happen along individual tubes rather than between adjacent tubes. The images clearly demonstrate that individually dispersed SWNTs are abundantly present in the solution.

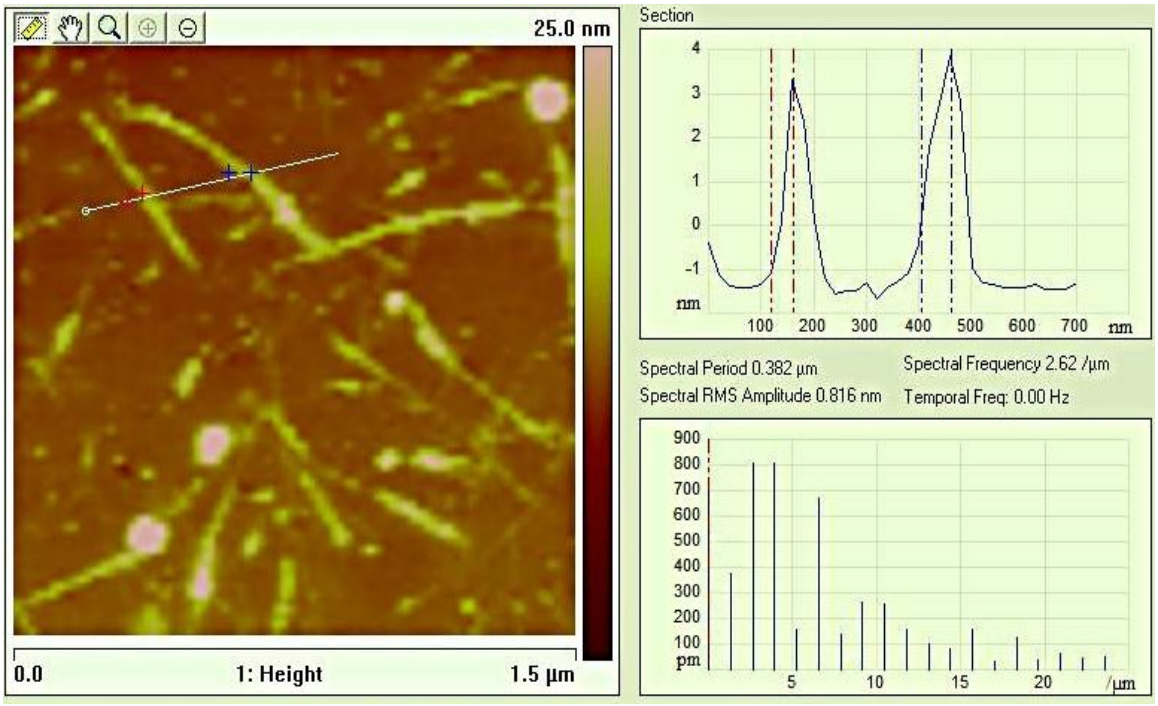

Figure 4.10. AFM image of polymer-wrapped SWNTs after crosslinking by GLU.

.

In this project we explored the adsorption of polymers onto SWNTs surfaces under aqueous conditions. Multiple types of non-covalent interactions play a role in this adsorption, including the interactions between the nanotube surface and solvent molecules, interactions between polymer and solvent molecules, the interactions between polymer molecules and the nanotube surface, and the interactions between solvent molecules. Of these, the unusually-strong interactions between the solvent molecules for water, dominated by hydrogen bonding, often outweigh the attractions between the solvent molecules and hydrophobic components, a phenomenon termed, "the hydrophobic effect." Often, this hydrophobic effect is of sufficient magnitude to make surfactant or polymer dispersed nanoparticles thermodynamically metastable rather than

true thermodynamic minima. In the present work, the polymer-wrapped SWNTs almost certainly fall into this category. The lack of change in SWNT fluorescence spectra upon crosslinking suggests that the polymer/nanotube interactions have not significantly changed as a result of the crosslinking, and thus should not have significantly shifted the system thermodynamically. The dramatic difference in behavior upon adding an organic solvent to the system after crosslinking, however, indicates that the system has been kinetically stabilized. The most likely explanation for this is that the cross-linked sheathes are so significantly sterically hindered from removal that the polymer/SWNT complex should be viewed as a single entity, much in the same way a rotaxane is.

The polymer-sheath approach described here should be generally applicable to a variety of systems. The crosslinking of adsorbates has already been a useful strategy for stabilizing other types of nanoparticles. For example, Xiaogang Peng's work on crosslinking surfactant molecules around quantum dots has been extremely successful.[239] This approach is a general strategy that could be used for any number of nanoparticle systems. Further modification of the adsorbates can conceivably allow, for example, the nanoparticle/polymer complex to be incorporated covalently into polymer matrices or covalent tethering of targeting biomolecules. In continuing work in the Ausman lab, crosslinking the wrapping polymer under semi-dilute conditions rather than the dilute conditions described in this dissertation has the potential to produce covalently-linked three-dimensional networks that may act as hydrogels or even aerogels.

CHAPTER 5

EPOXY/POLYHEDRAL OLIGOMERIC SILSESQUIOXANE NANOCOMPOSITES

This chapter contains the result and discussion concerning the preparation and characterization of epoxy/polyhedral oligomeric silsesquioxane (POSS) nanocomposites. The first part of the chapter includes the synthesis of the epoxy/POSS nanocomposites, whereas second part of the chapter deals with the study of thermomechanical and barrier properties to characterize the composite material.

5.1. Synthesis and Curing of Epoxy/POSS Nanocomposites

Epoxy/POSS composites were synthesized with the addition of different wt. % of POSS in EPON 862 and cured with isophorone diamine (IPDA). The detailed procedure is provided in section 3.3.7. The curing reaction was monitored by Raman spectroscopy.

The Raman spectrum of neat DGEBF contains the characteristic epoxide CH_2 stretching at 3008 cm^{-1}, strong aromatic C=C stretching at 1600 cm^{-1}, CH_2 stretching at 2923 cm^{-1}, aromatic ring C-H stretching at 3068 cm^{-1} and epoxide C-O-C stretching at 1264 cm^{-1} (overlapped with aromatic C-H bending vibration band). The glycidyl-POSS also shows a similar spectrum except aromatic C=C and C-H vibration bands (Figure 5.1). Since the peak of the epoxide group's C-O-C stretch overlaps the peaks of aromatic

C-H bend, the peak at 3008 cm^{-1} is used to monitor the epoxy groups in the composites. Figure 5.2 shows the Raman spectra of the control epoxy and of the resulting nanocoposites containing 0.25, 0.5, 1, 2, 3 and 5 wt. % of POSS after curing with IPDA at 200^{o}C. The epoxide C-O-C bands have virtually vanished for both controlled epoxy and POSS-containing nanocomposites, confirming the success of the crosslinking reaction.

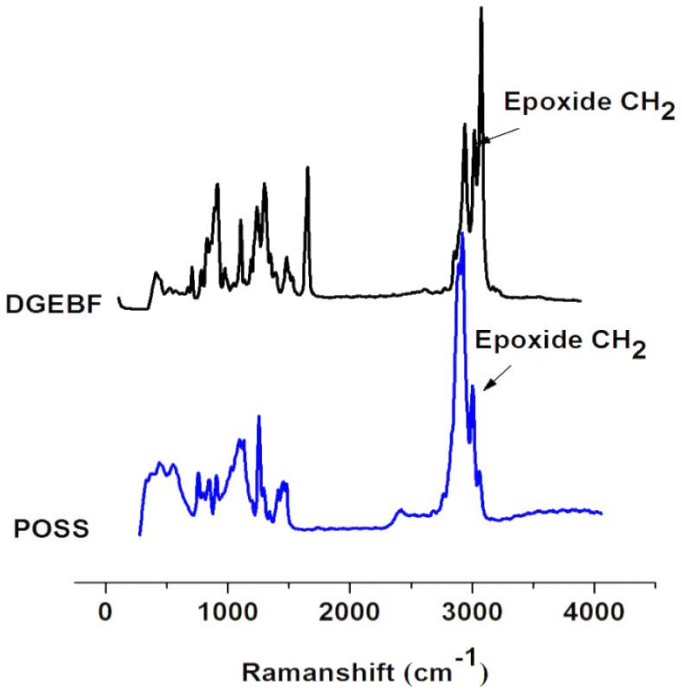

Figure 5.1. Raman spectra of DGEBF and POSS.

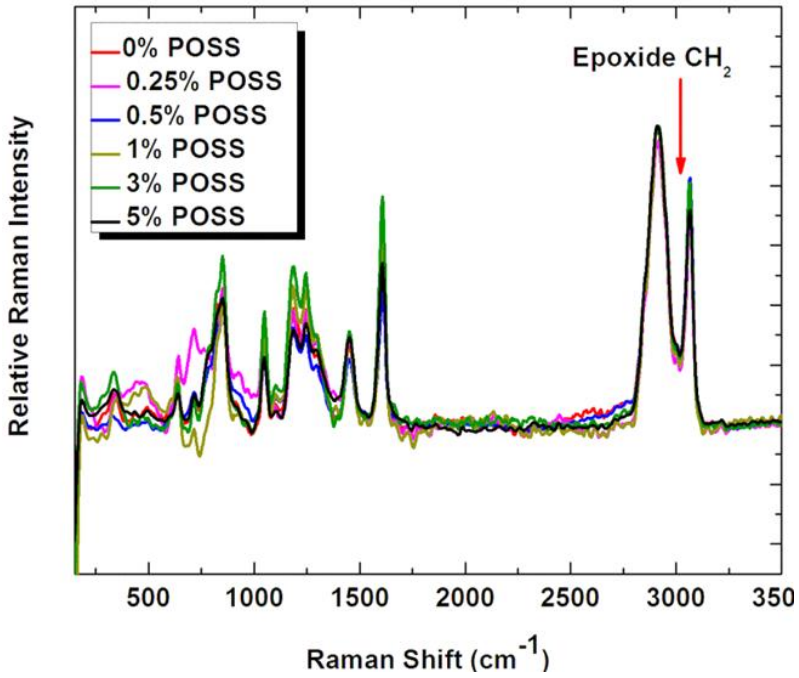

Figure 5.2. Raman spectra of Epoxy/POSS composites after post curing at 200^{o}C.

5.2. Characterization of Epoxy/POSS Nanocomposites

To study thermal, mechanical and barrier properties of the epoxy/POSS nanocomposites, samples containing the different POSS loadings were characterized by differential scanning calorimetry, dynamic mechanical analysis, fracture toughness measurements, and helium gas permeability tests.

5.2.1. Differential Scanning Calorimetry (DSC) Studies

The DSC thermal analysis results for the composites are presented in Figure 5.3. The control epoxy resin exhibits a glass transition temperature (T_g) of 126 ^{o}C. As POSS loading is increased, the T_g correspondingly increases to a maximum of 136 ^{o}C at a loading of 1 wt. % POSS, but then decreases slowly as the POSS loading increases above 1 wt. %. The initial increased in T_g reflects that the POSS is well-dispersed in the epoxy

resin, since in homogeneous dispersion the stiff silsesquioxanes tethers the soft organic chain of the epoxy matrix.[176] Thus, comparatively higher energy is required to move the molecular chain, increasing the T_g of the composites. In addition, the epoxy group present in the glycidyl-POSS also participates in the crosslinking reaction of the epoxy matrix. This reaction could lead to an increase in the crosslink density and thus an increase in $T_{g.}$ Above 1 wt. %, however, the POSS seems to undergo agglomeration, resulting in decreased T_g. Furthermore, higher concentrations of POSS will likely leave some residual uncrosslinked POSS which may acts as a lubricant within the epoxy system. This latter issue could be addressed in future studies by optimizing the amount of crosslinking agent added to account for the increased number epoxide groups present in the sample.

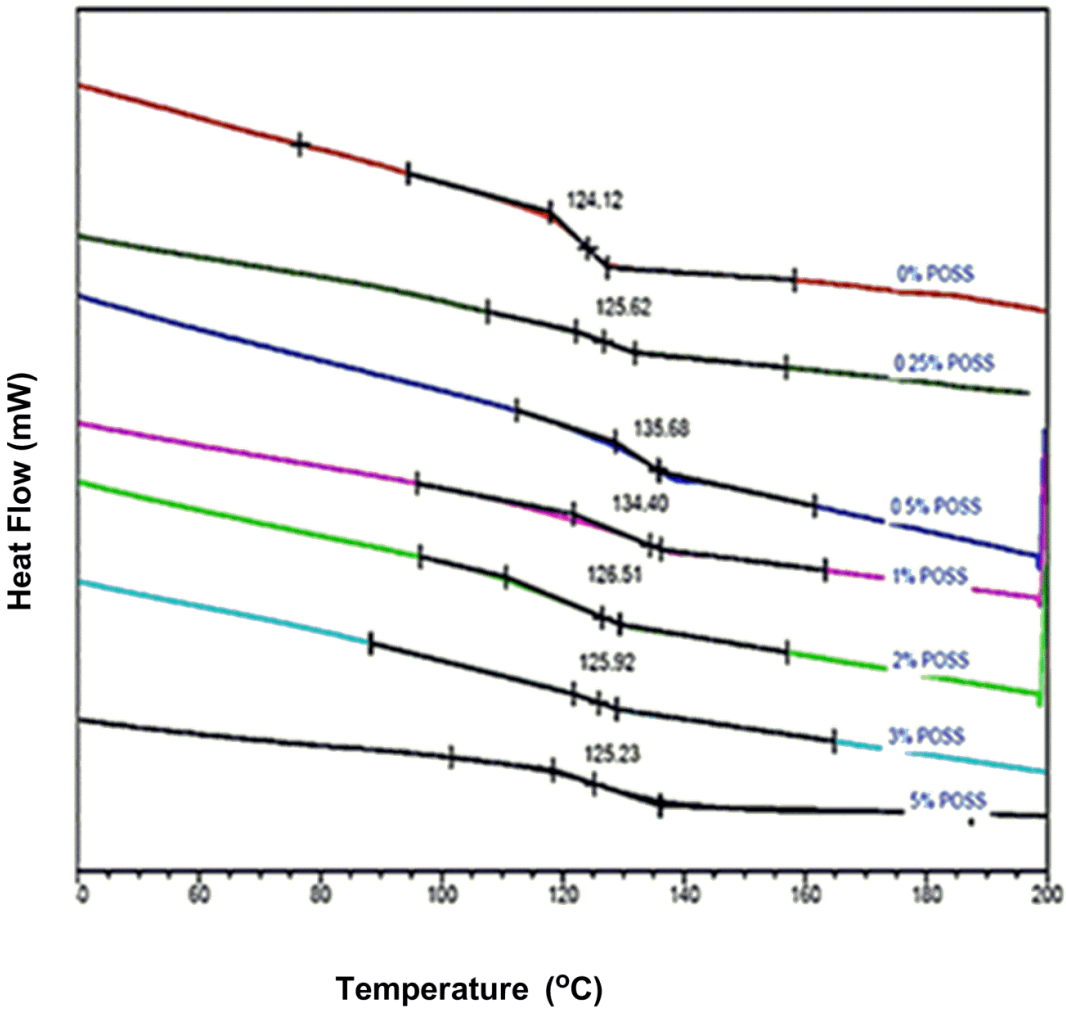

Figure 5.3. DSC curves for various epoxy/POSS composites.

5.2.2. Dynamic Mechanical Analysis (DMA)

Dynamic mechanical analysis is a very powerful technique to measure the viscoelastic properties of materials as they deform under periodic stress. Figure 5.4 shows the measurement of storage modulus as a function of temperature for various epoxy/POSS composites. This data clearly demonstrates that the storage modulus of epoxy/POSS composites are higher than that of neat epoxy resins at temperatures below the glass transition temperature. The storage modulus increases continuously up to

1 wt. % POSS loading, and then decreases with continued increases in POSS loading. This indicates that POSS cage has ability to reinforce into the epoxy resin but this ability decreases at higher POSS loading (>2 wt.%) because of poor dispersion and phase separation during polymerization.

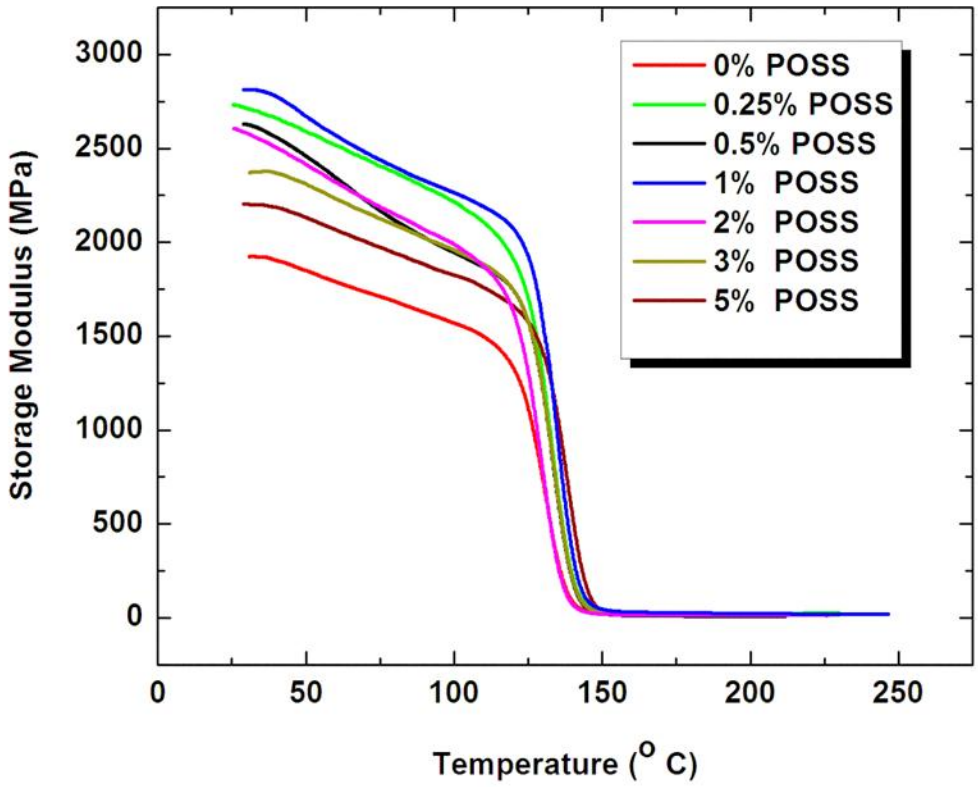

Figure 5.4. Plot of storage modulus vs temperature for epoxy/POSS composites.

Loss modulus measurements for the epoxy/POSS composites are presented in Figure 5.5. From this data it can be seen that the peak of loss modulus have shifted to higher temperature region in low concentration of POSS. Figure 5.6 is the plot of normalized tan delta as a function of temperature for various epoxy/POSS composites. The peak of the tan delta curve gives the T_g. The glass transition temperatures obtained

from this peak follow the same trend as do the results from DSC measurements. The T_g of the control epoxy resin as determined by DMA is 137.19 ^oC, which improves almost 9 ^oC for the composite having 1 wt. % of POSS. The comparison of T_g from DSC and DMA are presented in Figure 5.7.

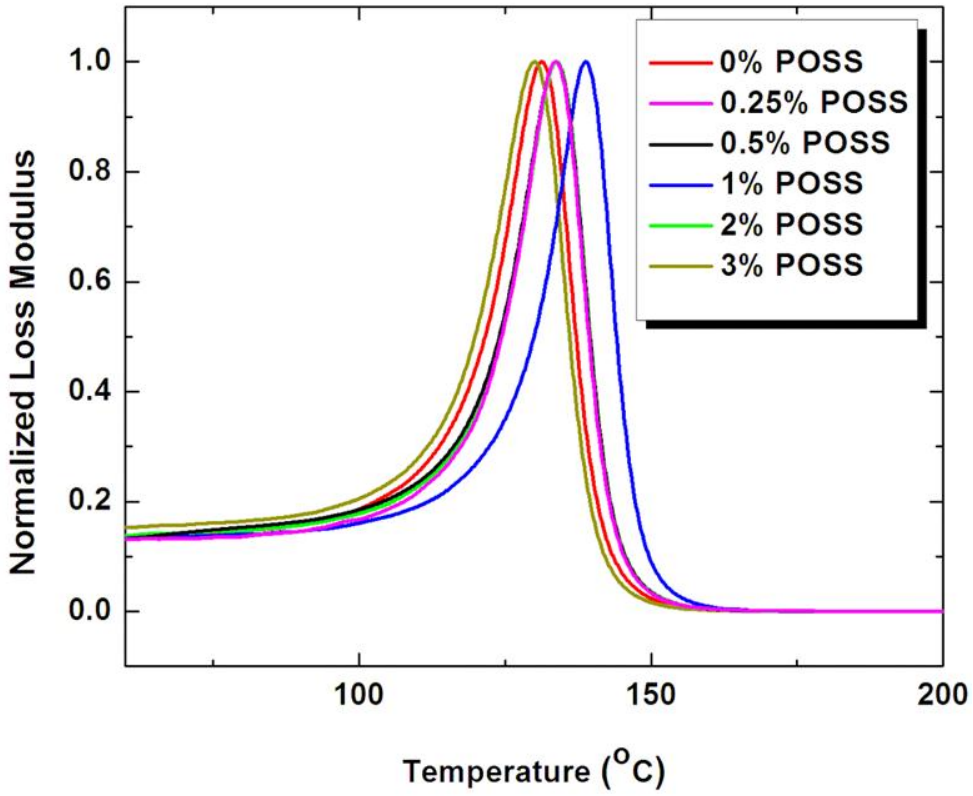

Figure 5.5. Loss modulus vs temperature curves for various epoxy/POSS composites.

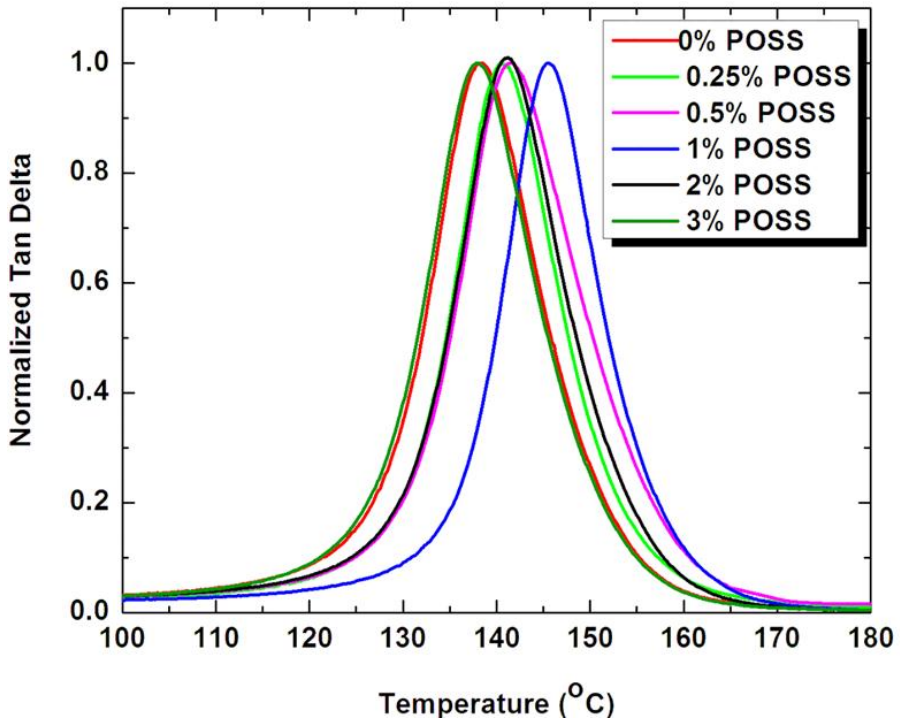

Figure 5.6. Tan delta curves for various epoxy/ POSS composites.

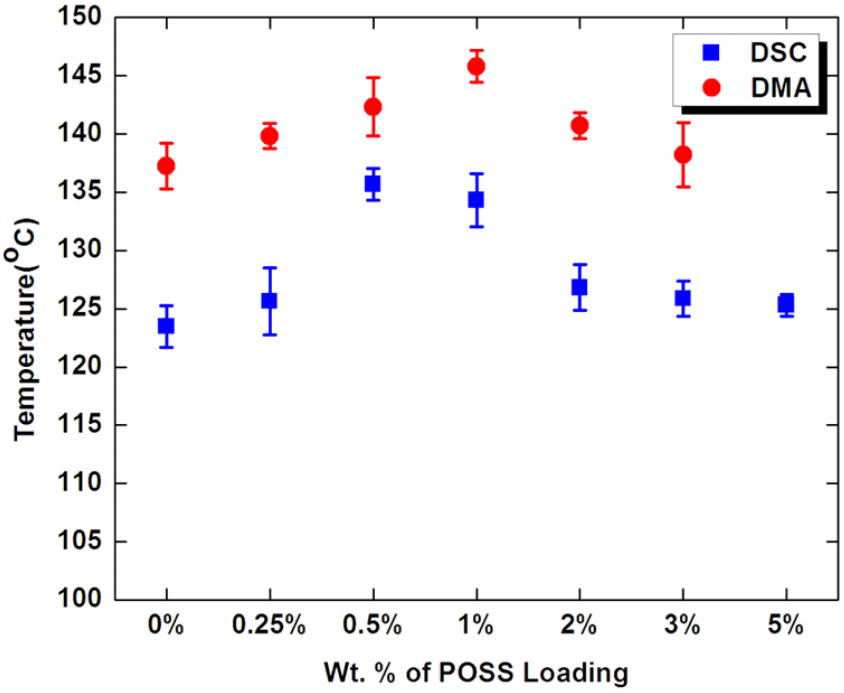

Figure 5.7. Comparison of T_g as determined by DSC and DMA.

5.2.3. Fracture Toughness

The fracture toughness of epoxy/POSS composites was evaluated by measuring critical stress intensity factor (K_{ic}). K_{ic} as of function of POSS content for the composites is presented in Figure 5.8. The K_{ic} value increases with the increase in the content of POSS up to 0.5 wt. %. The drop of the values of K_{ic} beyond 2 wt. % of POSS further supports the conclusion that the POSS could be aggregating at these high loadings. These agglomerates can act as weak sites, failing during crack initiation, thereby causing a decrease the values of K_{ic}.

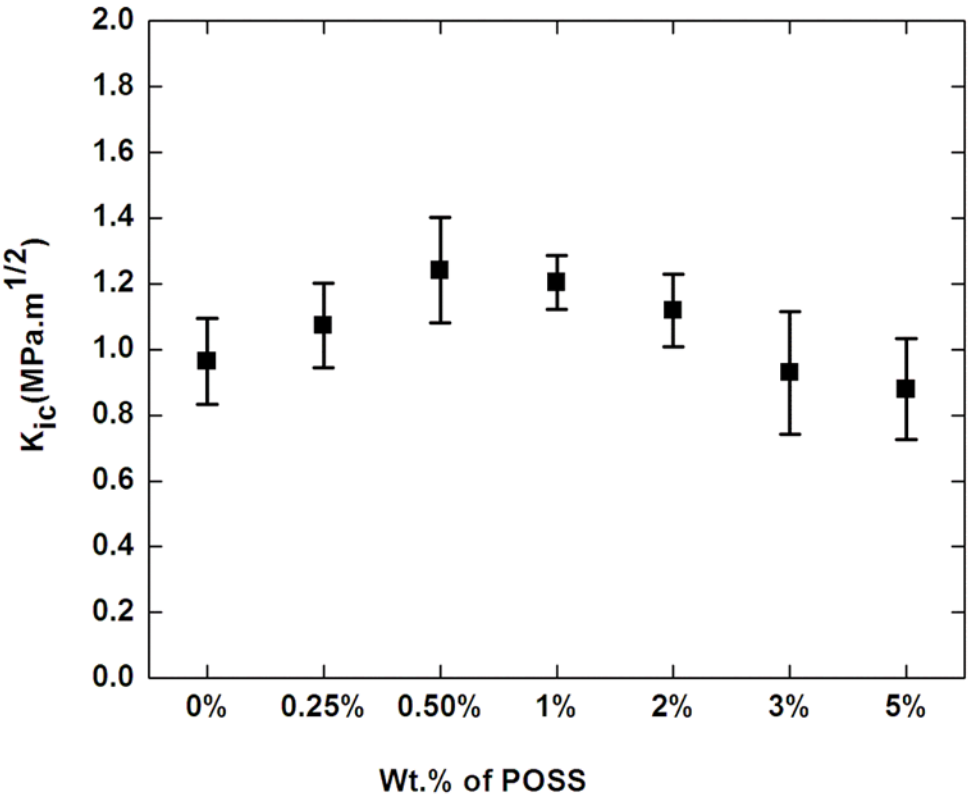

Figure 5.8. Fracture toughness value in term of critical intensity factors for different loading of POSS in epoxy/POSS composites.

The mechanism for fracture toughness improvement with the addition of a variety of fillers has been studied extensively for decades. Some of the well documented toughening mechanisms are crack deflection, plastic deformation, microcracking, void formation, and crack pinning.[240-243] To distinguish among these mechanism, the fracture surface morphology was characterized by SEM. Matrix cracking is clearly seen for the pure resin (Figure 5.9 a). On the other hand, epoxy/POSS composites have a comparatively rough surface (Figure 5.9 b and c). The formation of small microcracks is also observed on the fracture surface of 1 wt. % of POSS loading in the composites. However, as shown in Figure 5.9 c, both microcrack and macrocracks are observed in 5 wt. % of POSS loading. This result suggests that POSS might form aggregates and have a resulting heterogenous distribution at higher loading, which could result in the formation of macrocracks on the fracture surface. At higher magnification, the epoxy/POSS nanocomposites show some void formation due to the debonding of POSS nanoparticles (Figure 5.10). The size of these voids increases with increasing the amount of POSS, with the large voids created by the agglomerated POSS. Hence the fracture surfaces of the epoxy/POSS composite reveal that the increase in fracture toughness in low wt. % of POSS loading is caused by void formation and microcracking.

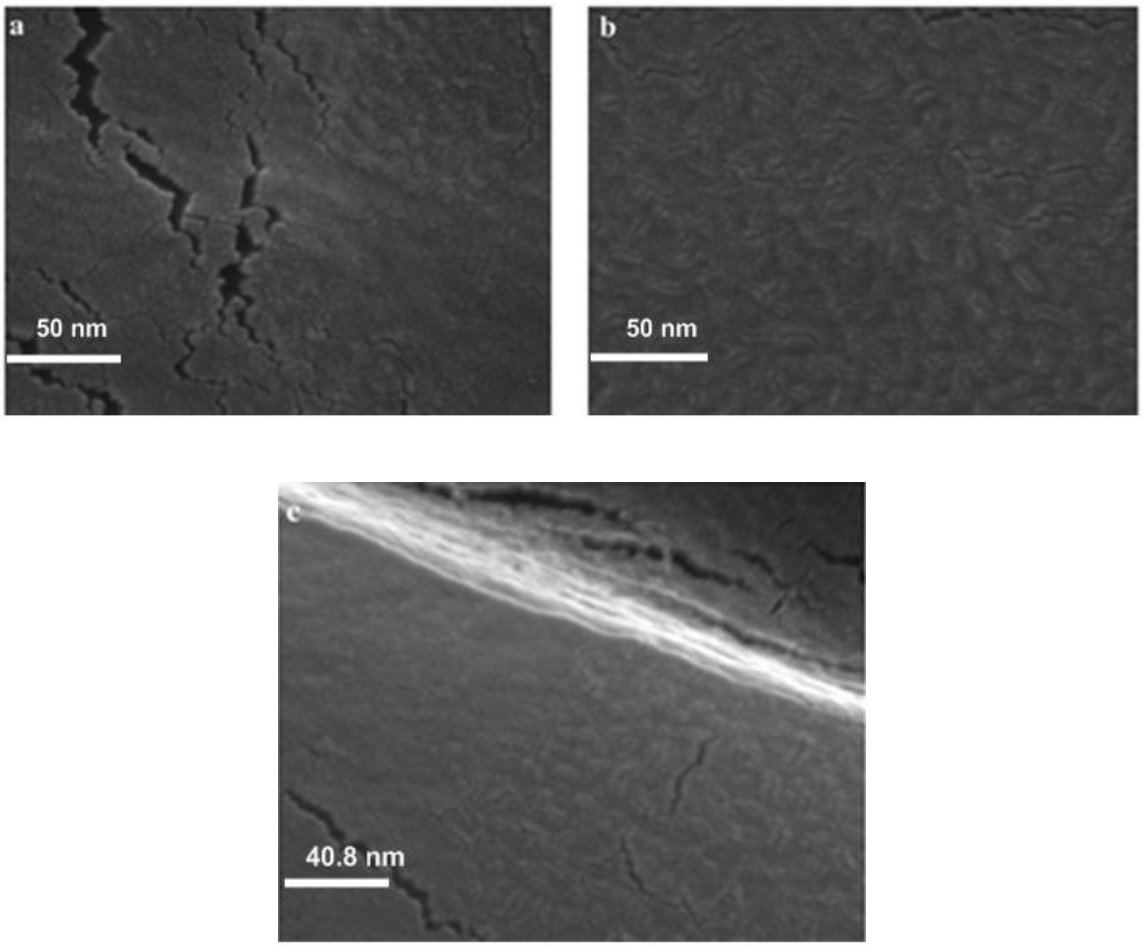

Figure 5.9. SEM micrographs of epoxy/POSS composites (a) neat resin (b) 1 wt.% POSS loading (c) 5 wt.% POSS loading.

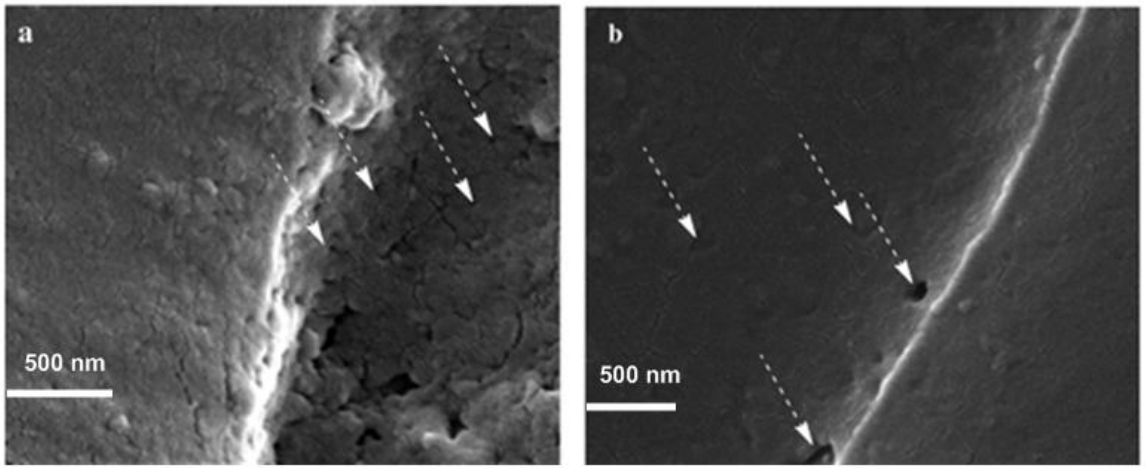

Figure 5.10. SEM micrographs of epoxy/POSS composites (a) 1 wt. % POSS loading (b) 5 wt.% POSS loading. Arrows point the formation of voids.

5.2.4. Helium Gas Permeability

The gas barrier properties of composite materials are measured in terms of a helium gas permeability coefficient. The data, presented in Figure 5.11, reveal that the incorporation of POSS in the epoxy resin dramatically improves the barrier properties of the thermoset up to a critical loading at which other tests indicated that agglomeration began to degrade the other properties of interest. The helium gas permeability is reduced by almost 70% on incorporation of 1 wt. % POSS into the neat epoxy resin. These results suggested that uniform dispersion of POSS is effective to increase the tortuosity of the diffusion path of the gas.

There are four possible pathways for gas transport through the epoxy POSS composites.

a) through the Si-O cage of POSS.

b) through the aggregate of POSS within polymer matrix

c) through the interface between POSS and Polymer matrix

d) through the polymer matrix

The process of insertion of molecular oxygen and nitrogen into POSS has been investigated theoretically by Tejerina *et al.*[244] They revealed that a high energy barrier exists in Si-O cage that prevents the permeation of the penetrant gas through it. Hence it is almost impossible to transport gases through Si-O cage of POSS. SEM images did not indicate the formation of POSS aggregation at lower wt. % of POSS. However, higher % POSS content in the composite can form the aggregate of POSS. Theses aggregate can provide tortuous pathways for the permeation of penetrant molecules, thereby increasing helium gas permeability of the composite material with higher wt. % of POSS (> 1 wt. %). Since there is significant increase in T_g in the composite materials at lower wt. % of POSS, there is clearly a strong interaction between the polymer matrix and the POSS molecules. In addition, there are eight epoxy groups on POSS cage structures that can also directly participate in the curing reaction and thus enhance the interaction between the two phases. This strong interaction between the polymer matrix and the POSS molecules reduces the formation of any interfacial gaps or void at the interface. Hence the permeation of gas through the interface is ruled out. The permeation of helium gas through the polymer matrix depends on the presence of excess free volume. Dispersion of POSS in the polymer matrix will cause reduction of the free volume and restriction of the polymer chain motion. Therefore, it will decrease the diffusivity and solubility of penetrant. This phenomenon explains the decrease in permeability compared to neat resin in case of POSS composites.

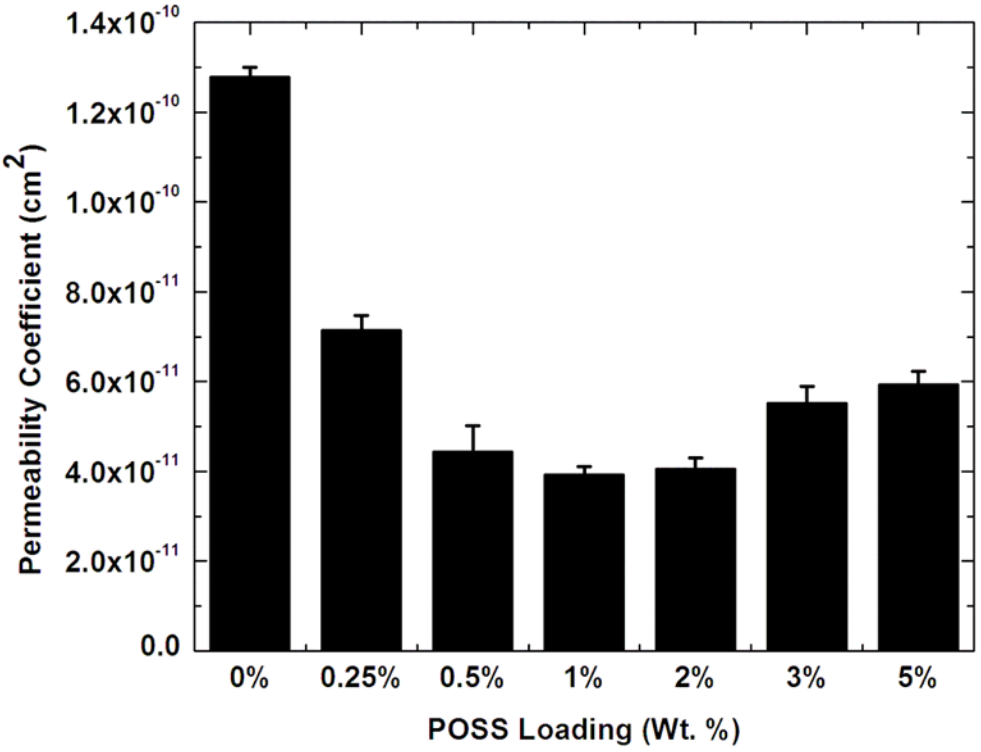

Figure 5.11. Helium gas permeability coefficient for epoxy composites at different POSS loading.

This project dealt with the use of nanofillers as polymer composite additives to improve the thermomechanical and gas permeability properties of nanocomposites. The final properties of the composite material depend not only on the properties of the individual component but also strongly depend upon the interfacial interaction between the nanofillers and polymer host. Many nanocomposite systems rely on weak intermolecular forces between the fillers and the polymer matrix, and thus are limited in the possible improvements that can be achieved, particularly with respect to gas permeability. Our system employed direct covalent crosslinking of the nanofiller into the polymer matrix to improve the key interfacial interactions. Up to the filler concentration

limit where filler aggregation began to play a significant role, at ca. 1 wt.%, this covalent incorporation resulted, as expected, in significant properties improvements. To improve the properties even further, techniques to further improve the filler dispersion throughout the matrix will need to be employed.

This approach is applicable to other polymer nanocomposites. The use of nanomaterial in polymer composite is not a new technology; however the optimization of the nanomaterial during processing is always challenging. This approach could be used as important tools to enhance the properties of nanocomposites in future. Due to the resulting high mechanical strength, low weight, high glass transition temperature, and low gas permeability, the particular composite developed in this work is especially appropriate for use in the manufacturing of carbon fiber reinforced composite fuel tanks.

CHAPTER 6

CONCLUSION

For the first research project we can conclude that uniform dispersion of SWNTs can be achieved by wrapping them with PVP and related crosslinkable copolymers like PVP-PAAm. However, SWNTs dispersion cannot be stabilized in different solvent system by wrapping them with PVP because of the detachment of the polymer. Our results demonstrate that crosslinking of PVP-PAAm by GLU before removing the SWNT/polymer complexes from their initial water environment can encapsulate SWNTs in individual, sealed shells. This method can stabilize the dispersion of SWNTs even against changing the solvent system. Our results open up the new possibility of isolated individual SWNTs that can now be transferred to a variety of solvent systems, and thus are suitable for a variety of applications, including as a filler for polymer composites.

In second research project we developed an epoxy nanocomposite with the addition of glycidyl-POSS that enhances the thermal, mechanical and barrier properties. Results suggested that good dispersion of POSS in the epoxy matrix is critical to improve the properties of the resin. In lower wt. % of POSS loading, the POSS molecules disperse

homogeneously throughout the matrix and enhance all properties of interest. However, loadings above 1% by weight results in the agglomeration of POSS, degrading the properties of the materials. We found a 70% reduction in gas permeability, almost 45% improvement in fracture toughness, and 10 ^{o}C increase in T_g of the epoxy resin with the addition of 1 wt. % of POSS.

REFERENCES

(1) Yang, W.; Peters, J. I.; Williams Iii, R. O. *Int. J. Pharm.* **2008**, *356*, 239.

(2) Hoet, P.; Bruske-Hohlfeld, I.; Salata, O. *J. Nanobiotechnol.* **2004**, *2*, 12.

(3) Oberdörster, G.; Oberdörster, E.; Oberdörster, J. *Environ. Health Perspect.* **2005**, *113*.

(4) Schmidt, G.; Malwitz, M. M. *Curr. Opin. Colloid Interface Sci.* **2003**, *8*, 103.

(5) Estroff, L. A.; Hamilton, A. D. *Chem. Mater.* **2001**, *13*, 3227.

(6) Moniruzzaman, M.; Winey, K. I. *Macromolecules* **2006**, *39*, 5194.

(7) Gangopadhyay, R.; De, A. *Chem. Mater.* **2000**, *12*, 608.

(8) Ramanathan, T.; Abdala, A. A.; Stankovich, S.; Dikin, D. A.; Herrera Alonso, M.; Piner, R. D.; Adamson, D. H.; Schniepp, H. C.; Chen, X.; Ruoff, R. S.; Nguyen, S. T.; Aksay, I. A.; Prud'Homme, R. K.; Brinson, L. C. *Nat. Nano* **2008**, *3*, 327.

(9) Nazar, L. F.; Zhang, Z.; Zinkweg, D. *J. Am. Chem. Soc.* **1992**, *114*, 6239.

(10) Vassiliou, J. K.; Ziebarth, R. P.; DiSalvo, F. J.; Rosenberg, A. *Chem. Mater.* **1990**, *2*, 738.

(11) Beecroft, L. L.; Ober, C. K. *Chem. Mater.* **1997**, *9*, 1302.

(12) Potts, J. R.; Dreyer, D. R.; Bielawski, C. W.; Ruoff, R. S. *Polymer* **2011**, *52*, 5.

(13) Kim, H.; Abdala, A. A.; Macosko, C. W. *Macromolecules* **2010**, *43*, 6515.

(14) LeBaron, P. C.; Wang, Z.; Pinnavaia, T. J. *Appl. Clay Sci.* **1999**, *15*, 11.

(15) Giannelis, E. P. *Adv. Mater.* **1996**, *8*, 29.

(16) Pavlidou, S.; Papaspyrides, C. D. *Prog. Polym. Sci.* **2008**, *33*, 1119.

(17) Sahoo, N. G.; Rana, S.; Cho, J. W.; Li, L.; Chan, S. H. *Prog. Polym. Sci.* **2010**, *35*, 837.

(18) Bauhofer, W.; Kovacs, J. Z. *Compos. Sci. Technol.* **2009**, *69*, 1486.

(19) Rahmat, M.; Hubert, P. *Compos. Sci. Technol.* **2011**, *72*, 72.

(20) Qian, H.; Greenhalgh, E. S.; Shaffer, M. S. P.; Bismarck, A. *J. Mater. Chem.* **2010**, *20*, 4751.

(21) Zhang, W.; Zhuang, X.; Li, X.; lin, Y.; Bai, J.; Chen, Y. *React. Funct. Polym.* **2009**, *69*, 124.

(22) Kannan, R. Y.; Salacinski, H. J.; Butler, P. E.; Seifalian, A. M. *Acc. Chem. Res.* **2005**, *38*, 879.

(23) Meng, Q.; Hu, J. *Compos. Part A-Appl. Sci. Manufact.* **2009**, *40*, 1661.

(24) Jordan, J.; Jacob, K. I.; Tannenbaum, R.; Sharaf, M. A.; Jasiuk, I. *Mater. Sci. Engin. A* **2005**, *393*, 1.

(25) Li, D.; Kaner, R. B. *J. Am. Chem. Soc.* **2005**, *128*, 968.

(26) Mulvihill, M. J.; Habas, S. E.; Jen-La Plante, I.; Wan, J.; Mokari, T. *Chem. Mater.* **2010**, *22*, 5251.

(27) Rozenberg, B. A.; Tenne, R. *Prog. Polym. Sci.* **2008**, *33*, 40.

(28) Iijima, S. *Nature* **1991**, *354*, 56.

(29) Ajayan, P. M. *Chem. Rev.* **1999**, *99*, 1787.

(30) Coleman, J. N.; Khan, U.; Blau, W. J.; Gun'ko, Y. K. *Carbon* **2006**, *44*, 1624.

(31) Thostenson, E. T.; Ren, Z.; Chou, T.-W. *Compos. Sci. Technol.* **2001**, *61*, 1899.

(32) Sinnott, S. B.; Andrews, R. *Crit. Rev. Solid State Mater. Sci.* **2001**, *26*, 145.

(33) Krishnan, A.; Dujardin, E.; Ebbesen, T. W.; Yianilos, P. N.; Treacy, M. M. J. *Phys. Rev. B* **1998**, *58*, 14013.

(34) Han, Z.; Fina, A. *Prog. Polym. Sci.* **2011**, *36*, 914.

(35) Serp, P.; Castillejos, E. *ChemCatChem* **2010**, *2*, 41.

(36) Aliev, A. E.; Baughman, R. H. *Nat Mater.* **2010**, *9*, 385.

(37) Liu, H.; Song, C.; Zhang, L.; Zhang, J.; Wang, H.; Wilkinson, D. P. *J. Power Sources* **2006**, *155*, 95.

(38) Liu, C.; Fan, Y. Y.; Liu, M.; Cong, H. T.; Cheng, H. M.; Dresselhaus, M. S. *Science* **1999**, *286*, 1127.

(39) Ando, T. *NPG Asia Mater.* **2009**, *1*, 17.

(40) Kataura, H.; Kumazawa, Y.; Maniwa, Y.; Umezu, I.; Suzuki, S.; Ohtsuka, Y.; Achiba, Y. *Synth. Met.* **1999**, *103*, 2555.

(41) O'Connell, M. J.; Bachilo, S. M.; Huffman, C. B.; Moore, V. C.; Strano, M. S.; Haroz, E. H.; Rialon, K. L.; Boul, P. J.; Noon, W. H.; Kittrell, C.; Ma, J.; Hauge, R. H.; Weisman, R. B.; Smalley, R. E. *Science* **2002**, *297*, 593.

(42) Akai, Y.; Saito, S. *Physica E: Low. Dimen. Syst. Nanostruct.* **2005**, *29*, 555.

(43) Saito, R.; Fujita, M.; Dresselhaus, G.; Dresselhaus, M. S. *Phys. Rev. B* **1992**, *46*, 1804.

(44) Hamada, N.; Sawada, S.-i.; Oshiyama, A. *Phys. Rev. Lett.* **1992**, *68*, 1579.

(45) Tanaka, K.; Okahara, K.; Okada, M.; Yamabe, T. *Chem. Phys. Lett.* **1992**, *191*, 469.

(46) Kelley, T. W.; Baude, P. F.; Gerlach, C.; Ender, D. E.; Muyres, D.; Haase, M. A.; Vogel, D. E.; Theiss, S. D. *Chem. Mater.* **2004**, *16*, 4413.

(47) Peet, J.; Kim, J. Y.; Coates, N. E.; Ma, W. L.; Moses, D.; Heeger, A. J.; Bazan, G. C. *Nat. Mater.* **2007**, *6*, 497.

(48) Coombs, B. A.; Rutter, S. R.; Goeta, A. E.; Sparkes, H. A.; Batsanov, A. S.; Beeby, A. *RSC Advances* **2012**, *2*, 1870.

(49) Landi, B. J.; Raffaelle, R. P.; Castro, S. L.; Bailey, S. G. *Progress in Photovoltaics: Research and Applications* **2005**, *13*, 165.

(50) Geng, J.; Zeng, T. *J. Am. Chem. Soc.* **2006**, *128*, 16827.

(51) Ren, S.; Bernardi, M.; Lunt, R. R.; Bulovic, V.; Grossman, J. C.; Gradečak, S. *Nano Lett.* **2011**, *11*, 5316.

(52) Lee, H. W.; Yoon, Y.; Park, S.; Oh, J. H.; Hong, S.; Liyanage, L. S.; Wang, H.; Morishita, S.; Patil, N.; Park, Y. J.; Park, J. J.; Spakowitz, A.; Galli, G.; Gygi, F.; Wong, P. H. S.; Tok, J. B. H.; Kim, J. M.; Bao, Z. *Nat Commun* **2011**, *2*, 541.

(53) Lipomi, D. J.; Vosgueritchian, M.; Tee, B. C. K.; Hellstrom, S. L.; Lee, J. A.; Fox, C. H.; Bao, Z. *Nat Nano* **2011**, *6*, 788.

(54) Barman, S. N.; LeMieux, M. C.; Baek, J.; Rivera, R.; Bao, Z. *ACS Applied Materials & Interfaces* **2010**, *2*, 2672.

(55) Dissanayake, N. M.; Zhong, Z. *Nano Lett.* **2010**, *11*, 286.

(56) Wilder, J. W. G.; Venema, L. C.; Rinzler, A. G.; Smalley, R. E.; Dekker, C. *Nature* **1998**, *391*, 59.

(57) Iijima, S.; Ichihashi, T. *Nature* **1993**, *363*, 603.

(58) Bethune, D. S.; Klang, C. H.; de Vries, M. S.; Gorman, G.; Savoy, R.; Vazquez, J.; Beyers, R. *Nature* **1993**, *363*, 605.

(59) Thess, A.; Lee, R.; Nikolaev, P.; Dai, H.; Petit, P.; Robert, J.; Xu, C.; Lee, Y. H.; Kim, S. G.; Rinzler, A. G.; Colbert, D. T.; Scuseria, G. E.; Tománek, D.; Fischer, J. E.; Smalley, R. E. *Science* **1996**, *273*, 483.

(60) Dai, H.; Dresselhaus, M., Dresselhaus, G., Avouris, P., Eds.; Springer Berlin / Heidelberg: 2001; Vol. 80, p 29.

(61) Dai, H. *Acc. Chem. Res.* **2002**, *35*, 1035.

(62) Tibbetts, G. G. *J. Cryst. Growth* **1984**, *66*, 632.

(63) Tibbetts, G. G. *Carbon* **1989**, *27*, 745.

(64) Huang, S.; Woodson, M.; Smalley, R.; Liu, J. *Nano Lett.* **2004**, *4*, 1025.

(65) Zheng, B.; Lu, C.; Gu, G.; Makarovski, A.; Finkelstein, G.; Liu, J. *Nano Lett.* **2002**, *2*, 895.

(66) Cassell, A. M.; Raymakers, J. A.; Kong, J.; Dai, H. *J. Phys. Chem. B* **1999**, *103*, 6484.

(67) Hata, K.; Futaba, D. N.; Mizuno, K.; Namai, T.; Yumura, M.; Iijima, S. *Science* **2004**, *306*, 1362.

(68) Yang, Q. H.; Bai, S.; Fournier, T.; Li, F.; Wang, G.; Cheng, H. M.; Bai, J. B. *Chem. Phys. Lett.* **2003**, *370*, 274.

(69) Nikolaev, P.; Bronikowski, M. J.; Bradley, R. K.; Rohmund, F.; Colbert, D. T.; Smith, K. A.; Smalley, R. E. *Chem. Phys. Lett.* **1999**, *313*, 91.

(70) Kitiyanan, B.; Alvarez, W. E.; Harwell, J. H.; Resasco, D. E. *Chem. Phys. Lett.* **2000**, *317*, 497.

(71) Alvarez, W. E.; Kitiyanan, B.; Borgna, A.; Resasco, D. E. *Carbon* **2001**, *39*, 547.

(72) Odom, T. W.; Huang, J.-L.; Kim, P.; Lieber, C. M. *J. Phys. Chem. B* **2000**, *104*, 2794.

(73) Kim, P.; Odom, T. W.; Huang, J.-L.; Lieber, C. M. *Phys. Rev. Lett.* **1999**, *82*, 1225.

(74) Mintmire, J. W.; White, C. T. *Phys. Rev. Lett.* **1998**, *81*, 2506.

(75) Bachilo, S. M.; Strano, M. S.; Kittrell, C.; Hauge, R. H.; Smalley, R. E.; Weisman, R. B. *Science* **2002**, *298*, 2361.

(76) Graupner, R. *J. Raman Spectrosc.* **2007**, *38*, 673.

(77) Dresselhaus, M. S.; Dresselhaus, G.; Saito, R.; Jorio, A. *Physics Reports* **2005**, *409*, 47.

(78) Souza Filho, A. G.; Chou, S. G.; Samsonidze, G. G.; Dresselhaus, G.; Dresselhaus, M. S.; An, L.; Liu, J.; Swan, A. K.; Ünlü, M. S.; Goldberg, B. B.; Jorio, A.; Grüneis, A.; Saito, R. *Phys. Rev. B* **2004**, *69*, 115428.

(79) Saito, R.; Dresselhaus, G.; Dresselhaus, M. S. *Phys. Rev. B* **2000**, *61*, 2981.

(80) Brown, S. D. M.; Jorio, A.; Corio, P.; Dresselhaus, M. S.; Dresselhaus, G.; Saito, R.; Kneipp, K. *Phys. Rev. B* **2001**, *63*, 155414.

(81) Jorio, A.; Souza Filho, A. G.; Dresselhaus, G.; Dresselhaus, M. S.; Swan, A. K.; Ünlü, M. S.; Goldberg, B. B.; Pimenta, M. A.; Hafner, J. H.; Lieber, C. M.; Saito, R. *Phys. Rev. B* **2002**, *65*, 155412.

(82) Jorio, A.; Fantini, C.; Dantas, M. S. S.; Pimenta, M. A.; Souza Filho, A. G.; Samsonidze, G. G.; Brar, V. W.; Dresselhaus, G.; Dresselhaus, M. S.; Swan, A. K.; Ünlü, M. S.; Goldberg, B. B.; Saito, R. *Phys. Rev. B* **2002**, *66*, 115411.

(83) Girifalco, L. A.; Hodak, M.; Lee, R. S. *Phys. Rev. B* **2000**, *62*, 13104.

(84) Ajayan, P. M.; Tour, J. M. *Nature* **2007**, *447*, 1066.

(85) Etika, K. C.; Cox, M. A.; Grunlan, J. C. *Polymer* **2010**, *51*, 1761.

(86) Maeda, Y.; Kimura, S.-i.; Hirashima, Y.; Kanda, M.; Lian, Y.; Wakahara, T.; Akasaka, T.; Hasegawa, T.; Tokumoto, H.; Shimizu, T.; Kataura, H.; Miyauchi, Y.; Maruyama, S.; Kobayashi, K.; Nagase, S. *J. Phys. Chem. B* **2004**, *108*, 18395.

(87) Wang, H. *Curr. Opin. Colloid Interface Sci.* **2009**, *14*, 364.

(88) Hu, H.; Ni, Y.; Montana, V.; Haddon, R. C.; Parpura, V. *Nano Lett.* **2004**, *4*, 507.

(89) Zhao, B.; Hu, H.; Haddon, R. C. *Adv. Funct. Mater.* **2004**, *14*, 71.

(90) Hamon, M. A.; Hui, H.; Bhowmik, P.; Itkis, H. M. E.; Haddon, R. C. *Appl. Phys. A-Mater.* **2002**, *74*, 333.

(91) Liu, M.; Yang, Y.; Zhu, T.; Liu, Z. *Carbon* **2005**, *43*, 1470.

(92) Kang, J.; Takhar, D.; Kuznetsov, O. V.; Khabashesku, V. N.; Kelly, K. F. *Chem. Phys. Lett.* **2012**, *534*, 43.

(93) Mickelson, E. T.; Huffman, C. B.; Rinzler, A. G.; Smalley, R. E.; Hauge, R. H.; Margrave, J. L. *Chem. Phys. Lett.* **1998**, *296*, 188.

(94) Bahr, J. L.; Tour, J. M. *Chem. Mater.* **2001**, *13*, 3823.

(95) Kooi, S. E.; Schlecht, U.; Burghard, M.; Kern, K. *Angew. Chem. Int. Ed.* **2002**, *41*, 1353.

(96) Sun, Y.; Wilson, S. R.; Schuster, D. I. *J. Am. Chem. Soc.* **2001**, *123*, 5348.

(97) Tagmatarchis, N.; Georgakilas, V.; Prato, M.; Shinohara, H. *Chem. Commun.* **2002**, 2010.

(98) Zhang, J.; Zou, H.; Qing, Q.; Yang, Y.; Li, Q.; Liu, Z.; Guo, X.; Du, Z. *J. Phys. Chem. B* **2003**, *107*, 3712.

(99) Balasubramanian, K.; Burghard, M. *Small* **2005**, *1*, 180.

(100) Qin, S.; Qin, D.; Ford, W. T.; Resasco, D. E.; Herrera, J. E. *Macromolecules* **2004**, *37*, 752.

(101) Yan, Y.; Cui, J.; Pötschke, P.; Voit, B. *Carbon* **2010**, *48*, 2603.

(102) Riggs, J. E.; Guo, Z.; Carroll, D. L.; Sun, Y.-P. *J. Am. Chem. Soc.* **2000**, *122*, 5879.

(103) Fu, K.; Huang, W.; Lin, Y.; Riddle, L. A.; Carroll, D. L.; Sun, Y.-P. *Nano Lett.* **2001**, *1*, 439.

(104) Martinez-Rubi, Y.; Guan, J.; Lin, S.; Scriver, C.; Sturgeon, R. E.; Simard, B. *Chem. Commun.* **2007**, 5146.

(105) Backes, C.; Hirsch, A. *Chemistry of Nanocarbons*; John Wiley & Sons, Ltd: 2010, p 1.

(106) Husanu, M.; Baibarac, M.; Baltog, I. *Physica E: Low. Dimen. Syst. Nanostruct.* **2008**, *41*, 66.

(107) Moore, V. C.; Strano, M. S.; Haroz, E. H.; Hauge, R. H.; Smalley, R. E.; Schmidt, J.; Talmon, Y. *Nano Lett.* **2003**, *3*, 1379.

(108) Lu, K. L.; Lago, R. M.; Chen, Y. K.; Green, M. L. H.; Harris, P. J. F.; Tsang, S. C. *Carbon* **1996**, *34*, 814.

(109) Matarredona, O.; Rhoads, H.; Li, Z.; Harwell, J. H.; Balzano, L.; Resasco, D. E. *J. Phys. Chem. B* **2003**, *107*, 13357.

(110) Strano, M. S.; Moore, V. C.; Miller, M. K.; Allen, M. J.; Haroz, E. H.; Kittrell, C.; Hauge, R. H.; Smalley, R. E. *J. Nanosci. Nanotechnol.* **2003**, *3*, 81.

(111) Meuer, S.; Braun, L.; Zentel, R. *Macromol. Chem. Phys.* **2009**, *210*, 1528.

(112) Lou, X.; Daussin, R.; Cuenot, S.; Duwez, A.-S.; Pagnoulle, C.; Detrembleur, C.; Bailly, C.; Jérôme, R. *Chem. Mater.* **2004**, *16*, 4005.

(113) Bahun, G. J.; Wang, C.; Adronov, A. *J. Polym. Sci., Part A: Polym. Chem.* **2006**, *44*, 1941.

(114) Yang, L.-P.; Pan, C.-Y. *Macromol. Chem. Phys.* **2008**, *209*, 783.

(115) Chen, R. J.; Zhang, Y.; Wang, D.; Dai, H. *J. Am. Chem. Soc.* **2001**, *123*, 3838.

(116) Zhang, J.; Lee, J. K.; Wu, Y.; Murray, R. W. *Nano Lett.* **2003**, *3*, 403.

(117) Murakami, H.; Nomura, T.; Nakashima, N. *Chem. Phys. Lett.* **2003**, *378*, 481.

(118) O'Connell, M. J.; Boul, P.; Ericson, L. M.; Huffman, C.; Wang, Y.; Haroz, E.; Kuper, C.; Tour, J.; Ausman, K. D.; Smalley, R. E. *Chem. Phys. Lett.* **2001**, *342*, 265.

(119) Star, A.; Stoddart, J. F.; Steuerman, D.; Diehl, M.; Boukai, A.; Wong, E. W.; Yang, X.; Chung, S.-W.; Choi, H.; Heath, J. R. *Angew. Chem.* **2001**, *113*, 1771.

(120) Zheng, M.; Jagota, A.; Semke, E. D.; Diner, B. A.; McLean, R. S.; Lustig, S. R.; Richardson, R. E.; Tassi, N. G. *Nat. Mater.* **2003**, *2*, 338.

(121) Zorbas, V.; Ortiz-Acevedo, A.; Dalton, A. B.; Yoshida, M. M.; Dieckmann, G. R.; Draper, R. K.; Baughman, R. H.; Jose-Yacaman, M.; Musselman, I. H. *J. Am. Chem. Soc.* **2004**, *126*, 7222.

(122) Chiu, C.-c.; Dieckmann, G. R.; Nielsen, S. O. *Peptide Sci.* **2009**, *92*, 156.

(123) Star, A.; Steuerman, D. W.; Heath, J. R.; Stoddart, J. F. *Angew. Chem. Int. Ed.* **2002**, *41*, 2508.

(124) Bonnet, P.; Gresil, M.; Bizot, H.; Riou, I.; Bertoncini, P.; Buleon, A.; Chauvet, O. *J. Nanopart. Res.* **2010**, *12*, 545.

(125) Alpatova, A. L.; Shan, W.; Babica, P.; Upham, B. L.; Rogensues, A. R.; Masten, S. J.; Drown, E.; Mohanty, A. K.; Alocilja, E. C.; Tarabara, V. V. *Water Res.* **2010**, *44*, 505.

(126) Bandyopadhyaya, R.; Nativ-Roth, E.; Regev, O.; Yerushalmi-Rozen, R. *Nano Lett.* **2001**, *2*, 25.

(127) Li, G.; Wang, L.; Ni, H.; Pittman, C. U. *J. Inorg. Organomet. Polym.* **2001**, *11*, 123.

(128) Baney, R. H.; Itoh, M.; Sakakibara, A.; Suzuki, T. *Chem. Rev.* **1995**, *95*, 1409.

(129) Laine, R. M.; Choi, J.; Lee, I. *Adv. Mater.* **2001**, *13*, 800.

(130) Choi, J.; Harcup, J.; Yee, A. F.; Zhu, Q.; Laine, R. M. *J. Am. Chem. Soc.* **2001**, *123*, 11420.

(131) Brown, J. F.; Vogt, L. H. *J. Am. Chem. Soc.* **1965**, *87*, 4313.

(132) Sprung, M. M.; Guenther, F. O. *J. Am. Chem. Soc.* **1955**, *77*, 3996.

(133) Herren, D.; Bürgy, H.; Calzaferri, G. *Helv. Chim. Acta* **1991**, *74*, 24.

(134) Feher, F. J.; Newman, D. A.; Walzer, J. F. *J. Am. Chem. Soc.* **1989**, *111*, 1741.

(135) Lichtenhan, J. D.; Otonari, Y. A.; Carr, M. J. *Macromolecules* **1995**, *28*, 8435.

(136) Schwab, J. J.; Lichtenhan, J. D. *Appl. Organomet. Chem.* **1998**, *12*, 707.

(137) Gilman, J. W.; Schlitzer, D. S.; Lichtenhan, J. D. *J. Appl. Polym. Sci.* **1996**, *60*, 591.

(138) Feher, F. J.; Weller, K. J. *Organometallics* **1990**, *9*, 2638.

(139) Zhang, C.; Laine, R. M. *J. Am. Chem. Soc.* **2000**, *122*, 6979.

(140) Lee, L.-H.; Chen, W. C. *Polymer* **2005**, *46*, 2163.

(141) Zheng, L.; Waddon, A. J.; Farris, R. J.; Coughlin, E. B. *Macromolecules* **2002**, *35*, 2375.

(142) Loy, D. A.; Shea, K. J. *Chem. Rev.* **1995**, *95*, 1431.

(143) Vollenberg, P. H. T.; Heikens, D. *Polymer* **1989**, *30*, 1656.

(144) Andrady, A. L.; Merkel, T. C.; Toy, L. G. *Macromolecules* **2004**, *37*, 4329.

(145) Devi, R. R.; Maji, T. K. *Ind. Eng. Chem. Res.* **2012**, *51*, 3870.

(146) Wu, J.; Mather, P. T. *Polym. Rev.* **2009**, *49*, 25.

(147) Feher, F. J.; Weller, K. J. *Inorg. Chem.* **1991**, *30*, 880.

(148) Lichtenhan, J. D. *Comments Inorg. Chem.* **1995**, *17*, 115.

(149) Laine, R. M. *J. Mater. Chem.* **2005**, *15*, 3725.

(150) Voigt, A.; Murugavel, R.; Roesky, H. W. *Organometallics* **1996**, *15*, 5097.

(151) Kuo, S.-W.; Chang, F.-C. *Prog. Polym. Sci.* **2011**, *36*, 1649.

(152) Devaux, E.; Rochery, M.; Bourbigot, S. *Fire Mater.* **2002**, *26*, 149.

(153) Xiao, S.; Nguyen, M.; Gong, X.; Cao, Y.; Wu, H.; Moses, D.; Heeger, A. J. *Adv. Funct. Mater.* **2003**, *13*, 25.

(154) Braun, D.; Heeger, A. J. *Appl. Phys. Lett.* **1991**, *58*, 1982.

(155) Lee, J.; Cho, H.-J.; Cho, N. S.; Hwang, D.-H.; Kang, J.-M.; Lim, E.; Lee, J.-I.; Shim, H.-K. *J. Polym. Sci., Part A: Polym. Chem.* **2006**, *44*, 2943.

(156) Zhang, C.; Bunning, T. J.; Laine, R. M. *Chem. Mater.* **2001**, *13*, 3653.

(157) Kim, K.-M.; Chujo, Y. *J. Polym. Sci., Part A: Polym. Chem.* **2001**, *39*, 4035.

(158) Pan, Q.; Chen, X.; Fan, X.; Shen, Z.; Zhou, Q. *J. Mater. Chem.* **2008**, *18*, 3481.

(159) Wu, H.; Gonsalves, K. E. *Adv. Mater.* **2001**, *13*, 670.

(160) Ali, M.; Hicks, A. E. R.; Hellewell, P. G.; Thoma, G.; Norman, K. E. *The FASEB J.* **2003**,*11*,330

(161) Carter, K. R.; DiPietro, R. A.; Sanchez, M. I.; Russell, T. P.; Lakshmanan, P.; McGrath, J. E. *Chem. Mater.* **1997**, *9*, 105.

(162) Krause, B.; Koops, G. H.; van der Vegt, N. F. A.; Wessling, M.; Wübbenhorst, M.; van Turnhout, J. *Adv. Mater.* **2002**, *14*, 1041.

(163) Yang, B.-h.; Xu, H.-y.; Yang, Z.-z.; Liu, X.-y. *J. Mater. Chem.* **2009**, *19*, 9038.

(164) Chen, W.-C.; Kuo, S.-W.; Lu, C.-H.; Jeng, U. S.; Chang, F.-C. *Macromolecules* **2009**, *42*, 3580.

(165) Chen, S.-C.; Kuo, S.-W.; Jeng, U. S.; Su, C.-J.; Chang, F.-C. *Macromolecules* **2009**, *43*, 1083.

(166) Fei, M.; Jin, B.; Wang, W.; Liu, L. *J. Polym. Res.* **2010**, *17*, 19.

(167) Carniato, F.; Bisio, C.; Gatti, G.; Boccaleri, E.; Bertinetti, L.; Coluccia, S.; Monticelli, O.; Marchese, L. *Angew. Chem. Int. Ed.* **2009**, *48*, 6059.

(168) Fu, H.; Yang, L.; Yuan, H.; Xiao, F.; Lo, Y. *J. Am. Oil Chem. Soc.* **2008**, *85*, 1087.

(169) Liu, H.; Pratasik, S. B.; Nishikawa, T.; Shida, T.; Tachibana, K.; Fujiwara, T.; Nagai, H.; Kobayashi, H.; Namikoshi, M. *ChemInform* **2005**, *36*, no.

(170) Lee, A.; Lichtenhan, J. D. *Macromolecules* **1998**, *31*, 4970.

(171) Mya, K. Y.; He, C.; Huang, J.; Xiao, Y.; Dai, J.; Siow, Y.-P. *J. Polym. Sci., Part A: Polym. Chem.* **2004**, *42*, 3490.

(172) Strachota, A.; Kroutilová, I.; Kovářová, J.; Matějka, L. *Macromolecules* **2004**, *37*, 9457.

(173) Xu, H.; Yang, B.; Gao, X.; Li, C.; Guang, S. *J. Appl. Polym. Sci.* **2006**, *101*, 3730.

(174) Kim, G. M.; Qin, H.; Fang, X.; Sun, F. C.; Mather, P. T. *J. Polym. Sci., Part B: Polym. Phys.* **2003**, *41*, 3299.

(175) Xiao, F.; Sun, Y.; Xiu, Y.; Wong, C. P. *J. Appl. Polym. Sci.* **2007**, *104*, 2113.

(176) Zhang, Z.; Liang, G.; Wang, X. *Polym. Bull.* **2007**, *58*, 1013.

(177) Chen, J.; Hamon, M. A.; Hu, H.; Chen, Y.; Rao, A. M.; Eklund, P. C.; Haddon, R. C. *Science* **1998**, *282*, 95.

(178) Hamon, M. A.; Chen, J.; Hu, H.; Chen, Y.; Itkis, M. E.; Rao, A. M.; Eklund, P. C.; Haddon, R. C. *Adv. Mater.* **1999**, *11*, 834.

(179) Niyogi, S.; Hamon, M. A.; Hu, H.; Zhao, B.; Bhowmik, P.; Sen, R.; Itkis, M. E.; Haddon, R. C. *Acc. Chem. Res.* **2002**, *35*, 1105.

(180) Mickelson, E. T.; Chiang, I. W.; Zimmerman, J. L.; Boul, P. J.; Lozano, J.; Liu, J.; Smalley, R. E.; Hauge, R. H.; Margrave, J. L. *J. Phys. Chem. B* **1999**, *103*, 4318.

(181) Holzinger, M.; Vostrowsky, O.; Hirsch, A.; Hennrich, F.; Kappes, M.; Weiss, R.; Jellen, F. *Angew. Chem. Int. Ed.* **2001**, *40*, 4002.

(182) Dyke, C. A.; Tour, J. M. *J. Phys. Chem. A* **2004**, *108*, 11151.

(183) Kakade, B. A.; Pillai, V. K. *Appl. Surf. Sci.* **2008**, *254*, 4936.

(184) Kim, W.-J.; Nair, N.; Lee, C. Y.; Strano, M. S. *J. Phys. Chem. C* **2008**, *112*, 7326.

(185) Peng, X.; Wong, S. S. *Adv. Mater.* **2009**, *21*, 625.

(186) Bouilly, D.; Cabana, J.; Meunier, F. O; Desjardins-Carrière, M.; Lapointe, F. O.; Gagnon, P.; Larouche, F. L.; Adam, E.; Paillet, M.; Martel, R. *ACS Nano* **2011**, *5*, 4927.

(187) Yuan, W.; Chan-Park, M. B. *ACS Appl. Mater. Interfaces* **2012**, *4*, 2065.

(188) Vijayakumar, C.; Balan, B.; Kim, M.-J.; Takeuchi, M. *J. Phys. Chem. C* **2011**, *115*, 4533.

(189) Britz, D. A.; Khlobystov, A. N. *Chem. Soc. Rev.* **2006**, *35*, 637.

(190) Liu, Y.; Gao, L.; Sun, J. *J. Phys. Chem. C* **2006**, *111*, 1223.

(191) Lin, Y.; Taylor, S.; Li, H.; Fernando, K. A. S.; Qu, L.; Wang, W.; Gu, L.; Zhou, B.; Sun, Y.-P. *J. Mater. Chem.* **2004**, *14*, 527.

(192) Moniruzzaman, M.; Winey, K. I. *Macromolecules* **2006**, *39*, 5194.

(193) Liu, J.; Rinzler, A. G.; Dai, H.; Hafner, J. H.; Bradley, R. K.; Boul, P. J.; Lu, A.; Iverson, T.; Shelimov, K.; Huffman, C. B.; Rodriguez-Macias, F.; Shon, Y.-S.; Lee, T. R.; Colbert, D. T.; Smalley, R. E. *Science* **1998**, *280*, 1253.

(194) Sinani, V. A.; Gheith, M. K.; Yaroslavov, A. A.; Rakhnyanskaya, A. A.; Sun, K.; Mamedov, A. A.; Wicksted, J. P.; Kotov, N. A. *J. Am. Chem. Soc.* **2005**, *127*, 3463.

(195) Chambers, G.; Carroll, C.; Farrell, G. F.; Dalton, A. B.; McNamara, M.; in het Panhuis, M.; Byrne, H. J. *Nano Lett.* **2003**, *3*, 843.

(196) Hu, C.; Zhang, Y.; Bao, G.; Zhang, Y.; Liu, M.; Wang, Z. L. *J. Phys. Chem. B* **2005**, *109*, 20072.

(197) Zheng, M.; Jagota, A.; Strano, M. S.; Santos, A. P.; Barone, P.; Chou, S. G.; Diner, B. A.; Dresselhaus, M. S.; Mclean, R. S.; Onoa, G. B.; Samsonidze, G. G.; Semke, E. D.; Usrey, M.; Walls, D. J. *Science* **2003**, *302*, 1545.

(198) Anilkumar, P.; Fernando, K. A. S.; Cao, L.; Lu, F.; Yang, F.; Song, W.; Sahu, S.; Qian, H.; Thorne, T. J.; Anderson, A.; Sun, Y.-P. *J. Phys. Chem. C* **2011**, *115*, 11010.

(199) Zheng, X.; Zhou, F. *J. X-Ray Sci. Technol.* **2011**, *19*, 275.

(200) Petrov, P.; Terlemezyan, L. In *Surface Modification of Nanotube Fillers*; Wiley-VCH Verlag GmbH & Co. KGaA: 2011, p 51.

(201) Harris, P. J. F. *Int. Mater. Rev.* **2004**, *49*, 31.

(202) Choi, S.; Sankar, B. V. *Compos. Part B: Eng.* **2008**, *39*, 782.

(203) Pearson, R. A.; Yee, A. F. *J. Mater. Sci.* **1989**, *24*, 2571.

(204) Yee, A. F.; Pearson, R. A. *J. Mater. Sci.* **1986**, *21*, 2462.

(205) Garg, A. C.; Mai, Y.-W. *Compos. Sci. Technol.* **1988**, *31*, 179.

(206) Pearson, R. A.; Yee, A. F. *J. Mater. Sci.* **1991**, *26*, 3828.

(207) Wise, C. W.; Cook, W. D.; Goodwin, A. A. *Polymer* **2000**, *41*, 4625.

(208) Ratna, D.; Banthia, A. *Macromol. Res.* **2004**, *12*, 11.

(209) Bucknall, C. B.; Partridge, I. K. *Polymer* **1983**, *24*, 639.

(210) Yoon, T. H.; Priddy, D. B.; Lyle, G. D.; McGrath, J. E. *Macromol. Symp.* **1995**, *98*, 673.

(211) Yoon, T.-H.; McGrath, J. E. *J. Appl. Polym. Sci.* **2001**, *80*, 1504.

(212) Ng, C. B.; Schadler, L. S.; Siegel, R. W. *Nanostruct. Mater.* **1999**, *12*, 507.

(213) Qi, B.; Zhang, Q. X.; Bannister, M.; Mai, Y. W. *Compos. Struct.* **2006**, *75*, 514.

(214) Kuo, D.-H.; Chang, C.-C.; Su, T.-Y.; Wang, W.-K.; Lin, B.-Y. *Mater. Chem. Phys.* **2004**, *85*, 201.

(215) Njuguna, J.; Pielichowski, K.; Alcock, J. R. *Adv. Eng. Mater.* **2007**, *9*, 835.

(216) Rana, S.; Alagirusamy, R.; Joshi, M. *J. Reinf. Plast. Compos.* **2009**, *28*, 461.

(217) Bekyarova, E.; Thostenson, E. T.; Yu, A.; Itkis, M. E.; Fakhrutdinov, D.; Chou, T.-W.; Haddon, R. C. *J. Phys. Chem. C* **2007**, *111*, 17865.

(218) Godara, A.; Mezzo, L.; Luizi, F.; Warrier, A.; Lomov, S. V.; van Vuure, A. W.; Gorbatikh, L.; Moldenaers, P.; Verpoest, I. *Carbon* **2009**, *47*, 2914.

(219) Kim, J. A.; Seong, D. G.; Kang, T. J.; Youn, J. R. *Carbon* **2006**, *44*, 1898.

(220) Ni, C.; Ni, G.; Zhang, S.; Liu, X.; Chen, M.; Liu, L. *Colloid Polym. Sci.* **2010**, *288*, 469.

(221) Ramírez, C.; Rico, M.; Torres, A.; Barral, L.; López, J.; Montero, B. *Eur. Polym. J.* **2008**, *44*, 3035.

(222) Sanchez, C.; Soler-Illia, G. J. d. A. A.; Ribot, F.; Lalot, T.; Mayer, C. R.; Cabuil, V. *Chem. Mater.* **2001**, *13*, 3061.

(223) Pan, G. *Physical Properties of Polymers Handbook;* Springer New York: **2007**, p 577.

(224) Wang, F.; Lu, X.; He, C. *J. Mater. Chem.* **2011**, *21*, 2775.

(225) Rashid, E. S. A.; Ariffin, K.; Kooi, C. C.; Akil, H. M. *Mater. Design* **2009**, *30*, 1.

(226) Xiao, F.; Sun, Y.; Xiu, Y.; Wong, C. P. *J. Appl. Polym. Sci.* **2007**, *104*, 2113.

(227) Li, G. Z.; Wang, L.; Toghiani, H.; Daulton, T. L.; Koyama, K.; Pittman, C. U. *Macromolecules* **2001**, *34*, 8686.

(228) Zhang, Y.; Lee, S.; Yoonessi, M.; Liang, K.; Pittman, C. U. *Polymer* **2006**, *47*, 2984.

(229) Su, C.-H.; Chiu, Y.-P.; Teng, C.-C.; Chiang, C.-L. *J. Polym. Res.* **2010**, *17*, 673.

(230) Liang, K.; Toghiani, H.; Pittman, C. *J. Inorg. Organomet. Polym. Mater.* **2011**, *21*, 128.

(231) Yoon, I.-N.; Lee, Y.; Kang, D.; Min, J.; Won, J.; Kim, M.; Soo Kang, Y.; Kim, S.-h.; Kim, J.-J. *Int. J. Adhes. Adhes.* **2011**, *31*, 119.

(232) Tanaka, K.; Chujo, Y. *J. Mater. Chem.* **2012**, *22*, 1733.

(233) Solovskii, M. V.; Nikol'skaya, N. V.; Korneeva, E. V.; Mikhailova, N. A.; Pavlov, G. M. *Russ. J. Appl. Chem.* **2001**, *74*, 663.

(234) Solovskii, M.; Nikol'skaya, N.; Zaikina, N. *Pharm. Chem. J.* **2002**, *36*, 7.

(235) ASTM D1434-82 (Re-approved 1992), Standard test method for determining gaspermeability characteristics of plastic film and sheeting, ASTM, **1992**. 203.

(236) Giordani, S.; Bergin, S. D.; Nicolosi, V.; Lebedkin, S.; Kappes, M. M.; Blau, W. J.; Coleman, J. N. *J. Phys. Chem. B* **2006**, *110*, 15708.

(237) Choi, J. H.; Strano, M. S. *Appl. Phys. Lett.* **2007**, *90*, 223114.

(238) Jeng, E. S.; Moll, A. E.; Roy, A. C.; Gastala, J. B.; Strano, M. S. *Nano Lett.* **2006**, *6*, 371.

(239) Guo, W.; Li, J. J.; Wang, A.; Peng, X. *J. Am. Chem. Soc.* **2003**, *125*, 3901.

(240) Huang, Y.; Hunston, D. L.; Kinloch Anthony, J.; Riew, C. K. In *Toughened Plastics I*; American Chemical Society: 1993; Vol. 233, p 1.

(241) Bagheri, R.; Marouf, B. T.; Pearson, R. A. *Polym. Rev.* **2009**, *49*, 201.

(242) Zhao, Q.; Hoa, S. V. *J. Compos. Mater.* **2007**, *41*, 201.

(243) Garg, A. C.; Mai, Y.-W. *Compos. Sci. Technol.* **1988**, *31*, 179.

(244) Tejerina, B.; Gordon, M. S. *J. Phys. Chem. B* **2002**, *106*, 11764.

VITA

LAWANYA RAJ OJHA

Candidate for the Degree of

Doctor of Philosophy

Thesis: TAILORING OF POLYMER-NANOMATERIAL INTERACTIONS

Major Field: Chemistry

Biographical:

Personal data: Born in Rajgadh, Jhapa, Nepal, on October 3, 1973.

Education: Graduated from Pashupati Secondary School, Nepal in July 1989, received Master of Science degree in Chemistry from Tribhuvan University, Kathmandu, Nepal in December 1999, received Master in Science degree in Chemistry from Western Illinois University, Macomb, IL in July 2007,completed the requirements for the Doctor of Philosophy in Chemistry at Oklahoma State University, Stillwater, OK in July 2012.

Experience: Lecturer in Little Angels' College, Lalitpur, Nepal 1999- 2005, Graduate Research Assistant, Department of Chemistry, Western Illinois University, Macomb, IL 2005-2007, Graduate Research Assistant, Department of Chemistry, Oklahoma State University, Stillwater, OK 2008-20012.

Professional Memberships: American Chemical Society

Name: Lawanya Raj Ojha Date of Degree: December, 2012

Institution: Oklahoma State University Location: Stillwater, Oklahoma

Title of Study: TAILORING OF POLYMER-NANOMATERIAL INTERACTIONS

Pages in Study: 90 Candidate for the Degree of Doctor of Philosophy

Major Field: Chemistry

Scope and Method of Study: The purpose of this research work is to investigate polymer nanomaterial interaction to understand the properties of the polymer nanocomposites. The first part of the dissertation explored the dispersion of single-walled carbon nanotubes (SWNTs) that are non-covalently wrapped with a crosslinkable polymer and stabilized for transfer to different solvent systems by crosslinking. This method can be employed in processing SWNTs for polymeric composites. The second part of the dissertation concerns the development of epoxy/polyhedral oligomeric silsesquiaxanes composite in order to enhance thermal, mechanical and barrier properties of the resin.

Findings and Conclusions: Wrapping of SWNTs with a poly(N-vinylpyrrolidone-co-allylamine) (PVP-PAAm) polymer gave stable dispersions of SWNTs in water. After crosslinking of polymer with gluteraldehyde, the dispersion of SWNTs was no longer limited to aqueous suspension. The presence of individual nanotubes before and after crosslinking of polymer was confirmed by fluorescence spectroscopy. Epoxy/POSS composites were synthesized by incorporating a very low weight fraction of glycidyl POSS into Epon 862 resin by simple mechanical mixing. We found that there is a significant reduction in gas permeability and an improvement in thermomechanical properties of the resin with the addition of 1 wt. % of POSS. However, loadings above 1% by weight results the agglomeration of POSS, which degrades the properties of the materials.

ADVISER'S APPROVAL: Kevin D. Ausman